1-15-2016

GAR22β regulates cell migration, sperm motility, and axoneme structure

Ivonne Gamper
Rheinisch-Westfälische Technische Hochschule Aachen

David Fleck
Rheinisch-Westfälische Technische Hochschule Aachen

Meltem Barlin
Rheinisch-Westfälische Technische Hochschule Aachen

Marc Spehr
Rheinisch-Westfälische Technische Hochschule Aachen

Sara El Sayad
Rheinisch-Westfälische Technische Hochschule Aachen

See next page for additional authors

GAR22β regulates cell migration, sperm motility, and axoneme structure

Ivonne Gamper[a,b], David Fleck[c], Meltem Barlin[a,b], Marc Spehr[c], Sara El Sayad[a,b], Henning Kleine[d], Sebastian Maxeiner[a,b], Carmen Schalla[a,b], Gülcan Aydin[a,b], Mareike Hoss[e], David W. Litchfield[f], Bernhard Lüscher[d], Martin Zenke[a,b], and Antonio Sechi[a,b]

[a]Institute for Biomedical Engineering, Department of Cell Biology, RWTH Aachen University Medical School, D-52074 Aachen, Germany; [b]Helmholtz Institute for Biomedical Engineering and [c]Institute for Biology II, Department of Chemosensation, RWTH Aachen University, D-52074 Aachen, Germany; [d]Institute of Biochemistry and Molecular Biology and [e]Electron Microscopy Facility, Uniklinik RWTH Aachen, D-52074 Aachen, Germany; [f]Department of Biochemistry, Schulich School of Medicine and Dentistry, University of Western Ontario, London, ON N6A 5C1, Canada

ABSTRACT **Spatiotemporal cytoskeleton remodeling is pivotal for cell adhesion and migration. Here we investigated the function of Gas2-related protein on chromosome 22 (GAR22β), a poorly characterized protein that interacts with actin and microtubules. Primary and immortalized GAR22β$^{-/-}$ Sertoli cells moved faster than wild-type cells. In addition, GAR22β$^{-/-}$ cells showed a more prominent focal adhesion turnover. GAR22β overexpression or its reexpression in GAR22β$^{-/-}$ cells reduced cell motility and focal adhesion turnover. GAR22β–actin interaction was stronger than GAR22β–microtubule interaction, resulting in GAR22β localization and dynamics that mirrored those of the actin cytoskeleton. Mechanistically, GAR22β interacted with the regulator of microtubule dynamics end-binding protein 1 (EB1) via a novel noncanonical amino acid sequence, and this GAR22β–EB1 interaction was required for the ability of GAR22β to modulate cell motility. We found that GAR22β is highly expressed in mouse testes, and its absence resulted in reduced spermatozoa generation, lower actin levels in testes, and impaired motility and ultrastructural disorganization of spermatozoa. Collectively our findings identify GAR22β as a novel regulator of cell adhesion and migration and provide a foundation for understanding the molecular basis of diverse cytoskeleton-dependent processes.**

Monitoring Editor
Julie Brill
The Hospital for Sick Children

Received: Jun 22, 2015
Revised: Nov 3, 2015
Accepted: Nov 6, 2015

INTRODUCTION

Cytoskeleton dynamics and cell adhesion are crucial for cell motility, a prerequisite for several biological processes, such as development and immune responses. Actin dynamics plays a key role in cell motility (Small *et al.*, 2002; Sechi and Wehland, 2004; Disanza *et al.*, 2005; Carlier and Pantaloni, 2007), although efficient cell motility also requires functional coordination with microtubule (MT) dynamics (Vasiliev *et al.*, 1970; Goldman, 1971; Liao *et al.*, 1995; Mikhailov *et al.*, 1998).

The functional interplay between actin and MTs is regulated at multiple levels. For instance, tubulin binds to active Rac1, and MT repolymerization leads to Rac1 activation (Best *et al.*, 1996; Waterman-Storer *et al.*, 1999). Active Rac1 functionally reciprocates by promoting MT growth, possibly through its downstream effector Pak1, which blocks the ability of stathmin/Op18 to destabilize MTs (Daub *et al.*, 2001). MTs can affect focal adhesion (FA) dynamics by promoting FA dissociation (Kaverina *et al.*, 1999; Ballestrem *et al.*, 2000; Krylyshkina *et al.*, 2002). MT-driven FA disassembly is counterbalanced by the stabilization of MTs by active Rho. In particular, mDia1, a member of the formin family and the main effector of Rho-GTP, induces the alignment of MTs along stress fibers and increases the number of stable MTs (Ishizaki *et al.*, 2001; Palazzo *et al.*, 2001).

This article was published online ahead of print in MBoC in Press (http://www.molbiolcell.org/cgi/doi/10.1091/mbc.E15-06-0426) on November 12, 2015.

Address correspondence to: Antonio Sechi (Antonio.Sechi@rwth-aachen.de).

Abbreviations used: BTB, blood–testis barrier; CH, calponin homology; EB1, end-binding protein 1; EBM, EB1-binding motif; ES, ectoplasmic specialization; GAR, Gas2 related; GAR22β, Gas2-related protein on chromosome 22; MACF1, microtubule actin cross-linking factor 1.

Furthermore, FAs capture MTs and stabilize them against depolymerization by nocodazole (Kaverina *et al.*, 1998). Active Rac1 also forms a complex with the MT +tip protein, CLIP-170, and the actin cross-linking protein, IQGAP1. Disruption of the interaction between IQGAP1 and active Rac1 impairs lamellipodial activity (Fukata *et al.*, 2002).

Much less is known about proteins that physically interconnect actin and MTs. The proteins bullous pemphigoid antigen 1 (BPAG1) and microtubule actin cross-linking factor 1 (MACF1; also known as ACF7) have a similar and complex domain structure consisting, in particular, of two amino-terminal calponin homology (CH) domains and one carboxy-terminal Gas2-related (GAR) domain, which interact with actin filaments and MTs, respectively (Byers *et al.*, 1995; Okuda *et al.*, 1999; Sun *et al.*, 2001; Jefferson *et al.*, 2007). Little is known about the function of BPAG1, although it has been observed that BPAG1$^{-/-}$ cells show defective cytoskeleton organization and cell motility (Guo *et al.*, 1995). MACF1 gene deletion results in less stable MTs and in MTs that are bent and no longer aligned with actin bundles (Kodama *et al.*, 2003; Wu *et al.*, 2008). Moreover, MT targeting of FAs, FA dynamics, and cell motility are impaired in MACF1$^{-/-}$ cells (Kodama *et al.*, 2003; Wu *et al.*, 2008). Similar alterations of MT architecture and dynamics have been described in *Drosophila* S2 cells lacking the MACF1 homologue Short Stop (Applewhite *et al.*, 2010). Finally, the lack of MACF1 and Short Stop also causes deficient MT organization and filopodia formation in neuronal cells (Sanchez-Soriano *et al.*, 2009).

Gas2-related protein on chromosome 22 (GAR22β) is, among the proteins that interact with actin and MTs, still poorly characterized, and its effect on cytoskeleton-driven biological processes remains unclear. GAR22β has an apparently unstructured C-terminal portion, which shares no homology with known proteins. Moreover, similar to MACF1 and Short Stop, the N-terminal portion of GAR22β consists of CH and GAR domains, and it colocalizes with actin filaments and MTs (Goriounov *et al.*, 2003). Of interest, GAR22β expression is regulated by thyroid hormone receptor signaling in hematopoietic cells (Gamper *et al.*, 2009). Observations showing that GAR22β binds to the plus-end protein end-binding protein 1 (EB1; Jiang *et al.*, 2012; Stroud *et al.*, 2014; this study) suggest that GAR22β could regulate cytoskeletal dynamics and, thus, cell motility. In this study, we identified a novel noncanonical EB1-binding sequence within the C-terminal portion of GAR22β. We also demonstrated that GAR22β regulates lamellipodia dynamics, FA turnover, and directional cell motility. Generation of a GAR22β-knockout (KO) mouse demonstrated that the lack of GAR22β severely impaired generation of motile spermatozoa and caused alteration of their axonemal ultrastructure.

RESULTS

GAR22β is crucial for the regulation of cell motility and focal adhesion turnover

To determine whether GAR22β regulates cell motility and adhesion, we used Sertoli cells isolated from wild-type (WT) and GAR22β$^{-/-}$ testes (see later discussion for details about the GAR22β$^{-/-}$ mouse). Sertoli cells expressed GAR22β (as well as its splice variant GAR22α) and the Sertoli cell marker WT1. As expected, neither GAR22α nor GAR22β was detected in knockout cells (Figure 1, A and B). It is important to note that despite the presence of both GAR22 transcripts, all murine tissues (including testes) and cells lines studied so far express only GAR22β (Goriounov *et al.*, 2003). Therefore all phenotypic changes at the cellular and tissue levels that we describe in this study are likely due only to the lack of GAR22β.

Sertoli cells seeded on glass coverslips showed well-developed actin and MT cytoskeletons (Figure 1C, a and c), focal adhesions (Figure 1Cb), and typical EB1 localization at MT +tips (Figure 1Cd). In addition, both wild-type and GAR22β$^{-/-}$ Sertoli cells were highly motile (Figure 1, D and E), as determined using a wound-healing assay. Of importance, the immortalization of both wild-type and GAR22β$^{-/-}$ Sertoli cells did not affect the expression of the Sertoli cell marker WT1 (Figure 1B) and their motility (Figure 1, D and E). Hence our Sertoli cell lines are suitable for studying the effect of GAR22β on actin- and MT-dependent processes such as cell motility and FA turnover.

We sought to determine whether GAR22β is important for Sertoli cell motility and adhesion. As shown in Figure 1F, GAR22β$^{-/-}$ Sertoli cells were significantly faster than wild-type cells. Ectopic expression of GAR22β in GAR22β$^{-/-}$ Sertoli cells restored the motile phenotype of wild-type cells (Figure 1F), demonstrating both the specificity of these observations and the involvement of GAR22β in the regulation of cell motility. To investigate the specificity/generality of our findings, we also analyzed the influence of GAR22β on the motility of two murine cell lines that are frequently used to study cell motility, NIH-3T3 and B16F1 cells. Very low endogenous GAR22β expression levels rendered NIH-3T3 and B16F1 cells ideally suited for ectopic expression analysis. In both B16F1 and NIH-3T3 cells, GAR22β overexpression caused a robust reduction of average speed, persistence, and directionality of their movement (Supplemental Figure S1, Supplemental Fig1A_SUP_video 1, and Supplemental Fig1B_SUP_video2). This effect was likely due to the formation of small and less persistent lamellipodia around the entire cell perimeter (Supplemental Figure S1B and Supplemental Fig1B_SUP_video2). Overall our findings strongly support a role for GAR22β in the regulation of cell motility.

Finally, given the effect of GAR22β on directional cell motility, we asked whether it also affected FA dynamics. We expressed red fluorescent protein (RFP)–tagged zyxin, a focal adhesion component, in wild-type and GAR22β$^{-/-}$ Sertoli cells and quantified FA dynamics using a previously developed algorithm (Würflinger *et al.*, 2011). Both FA assembly and disassembly rates were significantly higher in GAR22β$^{-/-}$ Sertoli cells (Figure 1, G and H), indicating that the regulation of cell motility by GAR22β is also due to a change in FA turnover. In addition, reexpression of GAR22β in GAR22β$^{-/-}$ Sertoli cells partly restored FA turnover to wild-type levels, resulting in a robust decrease of FA disassembly rate (Figure 1, G and H). Consistent with these data, fluorescence recovery after photo bleaching (FRAP) experiments, which determine the subcellular kinetics of a protein, showed that the mobile fraction of RFP-zyxin is reduced by the expression of GAR22β in GAR22β$^{-/-}$ Sertoli cells (0.62 ± 0.23 [n = 29] for GAR22β$^{-/-}$ cells vs. 0.38 ± 0.19 [n = 28] for GAR22β$^{-/-}$ cells expressing GAR22β; p = 0.0001). Taken together, our findings clearly indicate that GAR22β is important for the regulation of cell motility and focal adhesion turnover.

The CH and GAR domains determine differential GAR22β localization and dynamics

To define more precisely the role of GAR22β in the regulation of cell motility, it is essential to establish the molecular determinants of its localization and dynamics. For this purpose, we expressed green fluorescent protein (GFP)–tagged GAR22β in B16F1 and GAR22β$^{-/-}$ Sertoli cells. GAR22β-GFP colocalized with F-actin–rich structures such as stress fibers and filopodia (Figure 2A, a–f). Because GAR22β colocalizes fairly well with the actin cytoskeleton, we hypothesized that its dynamics may reflect that of actin. For this analysis, we selected cells that expressed low amounts of GFP-GAR22β to reduce

effects potentially caused by its overexpression. In line with the foregoing results, we found that the dynamics of GFP-GAR22β at microspikes, filopodia, and lamellipodia closely resembled that of the actin cytoskeleton (Figure 2B and Supplemental Fig2B_SUP_videos 3 and 4). Of interest, GAR22β kinetics at lamellipodia and stress fibers was similar, as determined by FRAP analysis of its mobile fraction (0.75 ± 0.25 [n = 9] for GAR22β at lamellipodia vs. 0.77 ± 0.19 [n = 16] for GAR22β at stress fibers; p = 0.95). Despite the ability of GAR22β to interact with MTs in vitro (Goriounov *et al.*, 2003), we could not observe MT-like localization of GAR22β.

Because the expression of the GAR domain of ACF7/MACF1 is sufficient for bundling MTs and stabilizing them against nocodazole (Sun *et al.*, 2001), we reasoned that the CH and GAR domains might be involved in the ability of GAR22β to regulate the structure and dynamics of MTs and cell motility. Hence we sought to determine the contribution of the CH and GAR domains to GAR22β localization and dynamics. Deletion of the CH domain abolished the colocalization of GAR22β with the actin cytoskeleton, causing GAR22β to localize along thick and curled structures (Figure 3A; see Supplemental Figure S5 for GAR22β deletion mutants). Another consequence of the expression of GAR22β_ΔCH was the alteration of MT cytoskeleton architecture and EB1 localization, resulting in the formation of MT bundles and redistribution of EB1 from MT +tips to the entire MT framework (Figure 3B). We observed a similar phenotype in NIH-3T3 and B16F1 cells (Supplemental Figure S2). The deletion of the GAR domain led to less prominent phenotypic changes. In particular, GAR22β_ΔGAR colocalized only with a subset of actin structures corresponding to large stress fibers (Figure 3A and Supplemental Figure S2). Of note, GAR22β_ΔGAR was mostly excluded from more dynamic actin structures, such as actin networks at the cell periphery (Figure 3A and Supplemental Figure S2). In GAR22β_ΔGAR-expressing cells, MT architecture and EB1 localization were not grossly affected (Figure 3B).

Because the ability of GAR22β to interact with actin or MTs clearly influences its subcellular localization, we determined the contribution of the CH and GAR domains to the dynamics and kinetics of GAR22β. By using total internal reflection fluorescence (TIRF) microscopy and FRAP analysis, we found that the thick and curled GAR22β_ΔCH bundles were not static but showed lateral oscillations and occasional episodes of grow and shrinkage of their tips (Figure 3C and Supplemental Fig3CD_video5). Significantly, MT architecture and dynamics largely reflected that of GAR22β_ΔCH (Supplemental Figure S3 and Supplemental Fig3_SUP_video6). In contrast to GAR22β_ΔCH, GAR22β_ΔGAR appeared to be remarkably stable and showed little dynamic behavior (Figure 3D and Supplemental Fig3CD_video5). Consistent with these observations, FRAP experiments showed that the kinetics of GAR22β_ΔCH was faster than that of GAR22β_ΔGAR (Figure 3, E–I, and Supplemental Fig3_SUP_video7). Finally, we determined the influence of GAR22β-ΔCH and GAR22β-ΔGAR mutants on the motility of Sertoli and NIH-3T3 cells, using a wound-healing assay. The deletion of the CH or the GAR domain resulted in the mitigation of the effect of GAR22β on cell motility. In particular, the motility of GAR22β$^{-/-}$ Sertoli cells expressing GAR22β-ΔGAR was not significantly different from that of control GAR22β$^{-/-}$ cells and higher than that of wild-type Sertoli cells (Supplemental Figure 4A; compare to dashed line). We observed a minor decrease (compared with GAR22β$^{-/-}$ Sertoli cells) of the motility of GAR22β$^{-/-}$ Sertoli cells expressing GAR22β-ΔCH, although these cells, like Sertoli cells expressing GAR22β-ΔGAR, were clearly faster than wild-type Sertoli cells (Supplemental Figure 4B; compare to dashed line). Similarly, NIH-3T3 cells expressing GAR22β-ΔCH or GAR22β-ΔGAR were significantly faster than cells expressing full-length GAR22β, although both deletion mutants caused a reduction of average cell speed (Supplemental Figure 4C). Thus GAR22β modulation of cell motility requires binding to both actin filaments and MTs.

GAR22β directly binds to EB1 through a novel noncanonical sequence

To identify new binding partners of GAR22β, we applied tandem affinity purification and mass spectrometry analysis (Supplemental Figure 5A). Both GAR22β and its C-terminal portion, but not its N-terminal portion (GAR22α), directly bound to EB1 in a binding assay using purified proteins (Supplemental Figure 5B). These findings were corroborated using an inducible system in which the expression of GAR22β or its C-terminal portion was driven by the addition of doxycycline. By using an anti-GAR22 antibody, we found that EB1 coprecipitated with both GAR22β and GAR22β-COOH (Supplemental Figure 5C). The association between GAR22β and EB1 was specific, as indicated by the fact that on using an unrelated antibody or in the absence of doxycycline stimulation, we could not detect EB1 in GAR22β immunoprecipitates (Supplemental Figure 5C). Moreover, neither intact actin nor MT cytoskeletons are required for the formation of EB1–GAR22β complex (Supplemental Figure 5, D and E). During the finalization of this study, two studies appeared showing that GAR22β interacts with EB1 (Jiang *et al.*, 2012; Stroud *et al.*, 2014), thus supporting our findings.

Because deletion of the SxIP sequence does not abolish the interaction of GAR22β with EB1 (Stroud *et al.*, 2014), we reasoned that one or more additional EB1-binding sites could be present within the C-terminal portion of GAR22β. To test this hypothesis, we generated a panel of GAR22β deletion mutants (Figure 4A) and tested their binding to EB1 in vitro. We initially deleted the classical EB1-binding site SxIP and found that GAR22β was still able to associate with EB1 (GAR22β-589; Figure 4B). By generating shorter versions of GAR22β by progressive deletions of its C-terminal portion (Figure 4, A and B), we identified a noncanonical EB1-binding sequence between amino acids 347 and 357 (GAR22β-ΔEBM [for EB1-binding motif]; Figure 4, A and B), which is conserved in mouse and human GAR22β. We then examined the binding properties of some GAR22β variants in the context of physiological cytoplasmic interactions. Cells expressing the N-terminal portion of GAR22β (GAR22α) or full-length GAR22β served as negative and positive controls, respectively. Deletion of the CH domain did not influence GAR22β interaction with EB1, whereas the lack of the GAR domain reduced the ability of GAR22β to interact with EB1 (Figure 4C). Of note, deletion of the noncanonical EB1-binding site caused a fourfold reduction in the binding to EB1 compared with full-length GAR22β (Figure 4C). Furthermore, deletion of the SxIP motif resulted in nondetectable GAR22β–EB1 interactions, suggesting that interactions between GAR22β and EB1 mediated by the noncanonical motif are weaker, more transient, or a combination thereof (Figure 4C). Finally, we validated these findings by demonstrating that the C-terminal portion of GAR22β lacking the SxIP motif still colocalized with EB1 (Figure 4D). Of note, the deletion of the SxIP motif did not completely abolish the ability of GAR22β C-terminal portion to localize to MT +tips (Figure 4E; the localization of Cterm_ΔSxIP at MT +tips can be better appreciated in Supplemental Fig4E_video10). Our findings thus demonstrate that GAR22β binds specifically to EB1 via both a novel noncanonical sequence and a classical SxIP site.

GAR22β guides growing MTs along polarized actin filaments

The actin cytoskeleton guides growing MTs toward the cell periphery (Rodriguez *et al.*, 2003). Because GAR22β binds to actin

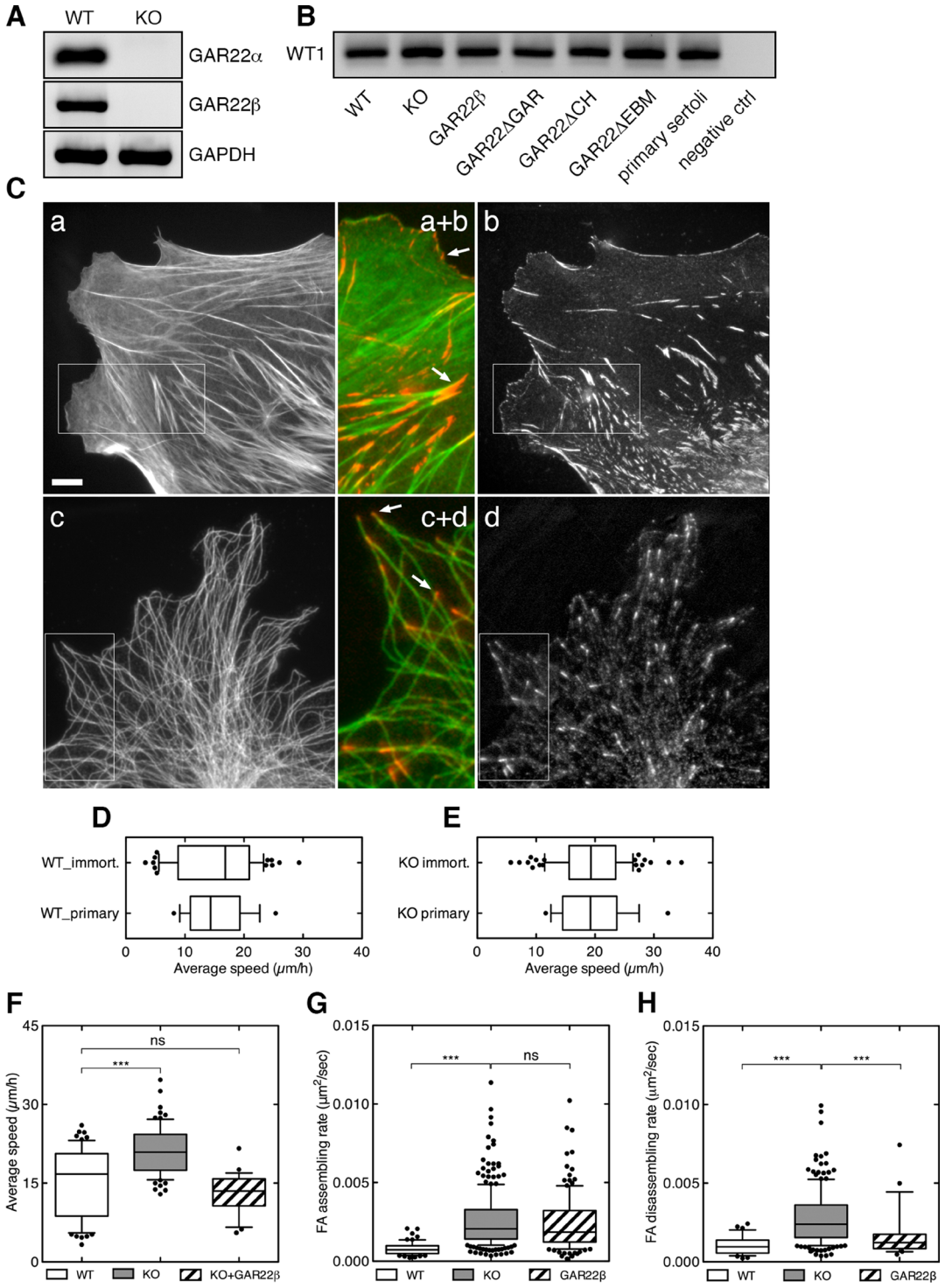

FIGURE 1: GAR22β is crucial for the regulation of cell motility and focal adhesion turnover. (A) Reverse transcription (RT)-PCR analysis of GAR22α and GAR22β expression in Sertoli cells isolated from wild-type or GAR22β$^{-/-}$ mice. Glyceraldehyde-3-phosphate dehydrogenase (GAPDH) served as loading control. (B) RT-PCR showing the expression of the Sertoli-specific marker WT1 in all Sertoli cell lines used in this study. (C) Normal architecture and distribution of actin filaments (a), focal adhesions (b), microtubules (c), and EB1 (d) in Sertoli cells. Sertoli cells were plated on glass coverslips, fixed, and labeled with fluorescent phalloidin (a) and antibodies against vinculin (b) or with anti-tubulin (c) and anti-EB1 (d) antibodies. Colored images show enlarged views of the boxed areas in a–d. Scale bar, 10 μm. (D, E) Immortalization of wild-type and GAR22β$^{-/-}$ Sertoli cells does not alter their motility. Graphs show average speed values as determined from wound-healing assays. In the box-and-whisker plots, the line in the middle of the box indicates the median, the top of the box indicates the 75th quartile, and the bottom of the box indicates the 25th quartile. Whiskers represent the 10th (lower) and 90th (upper) percentiles. (F–H) GAR22β is crucial for regulation of cell motility and focal adhesion turnover. (F) Analysis of Sertoli cell motility, showing that GAR22β$^{-/-}$ cells move significantly faster than wild-type cells. Expression of GAR22β in GAR22β$^{-/-}$ cells restores motility to wild-type levels, indicating

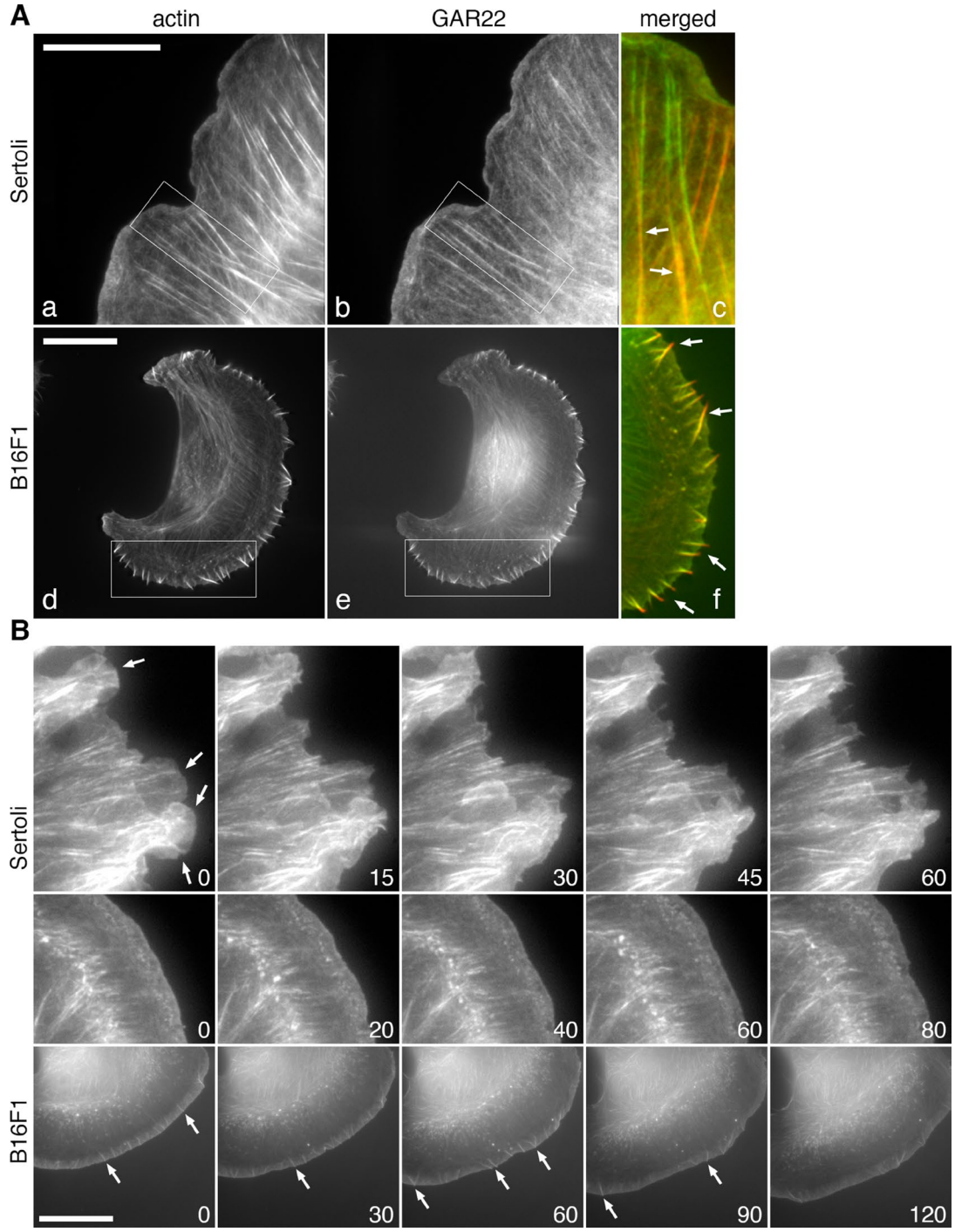

FIGURE 2: GAR22β colocalizes with the actin cytoskeleton and mimics actin dynamics in Sertoli and B16F1 cells. (A) Subcellular localization of GAR22β in Sertoli and B16F1 cells. Cells expressing GFP-GAR22β were fixed and labeled with fluorescent phalloidin. (a, d) Actin labeling (pseudocolored in red); (b, e) GFP-GAR22β (pseudocolored in green). GAR22β clearly colocalized with actin-rich structures such as stress fibers (arrows in c) and filopodia (arrows in f). Scale bars, 5 μm (a, b), 2.5 μm (c), 5 μm (d, e), 2.5 μm (f). (B) Dynamics of GFP-GAR22β in Sertoli and B16F1 cells. Top, middle, GFP-GAR22β dynamics in Sertoli cells; bottom, GFP-GAR22β dynamics in B16F1 cells. Note the localization of GAR22β at the fine actin meshwork at the leading edge in Sertoli (top, arrows) and B16F1 cells (bottom, arrows). Arrows in bottom images point to some filopodia in B16F1 cells. Numbers in the right corner of each image indicate elapsed time in seconds. Scale bar, 2 μm.

specific involvement of GAR22β in the regulation of this process. (G, H) Analysis of focal adhesion assembly (G) and disassembly (H) in Sertoli cells. Compared with wild-type cells, both FA assembly and disassembly rates were higher in GAR22β$^{-/-}$ cells. Of note, expression of GAR22β in GAR22β$^{-/-}$ cells restores FA disassembly rate to wild-type level but has no effect on FA assembly rate. ***$p < 0.0001$; ns, nonsignificant difference.

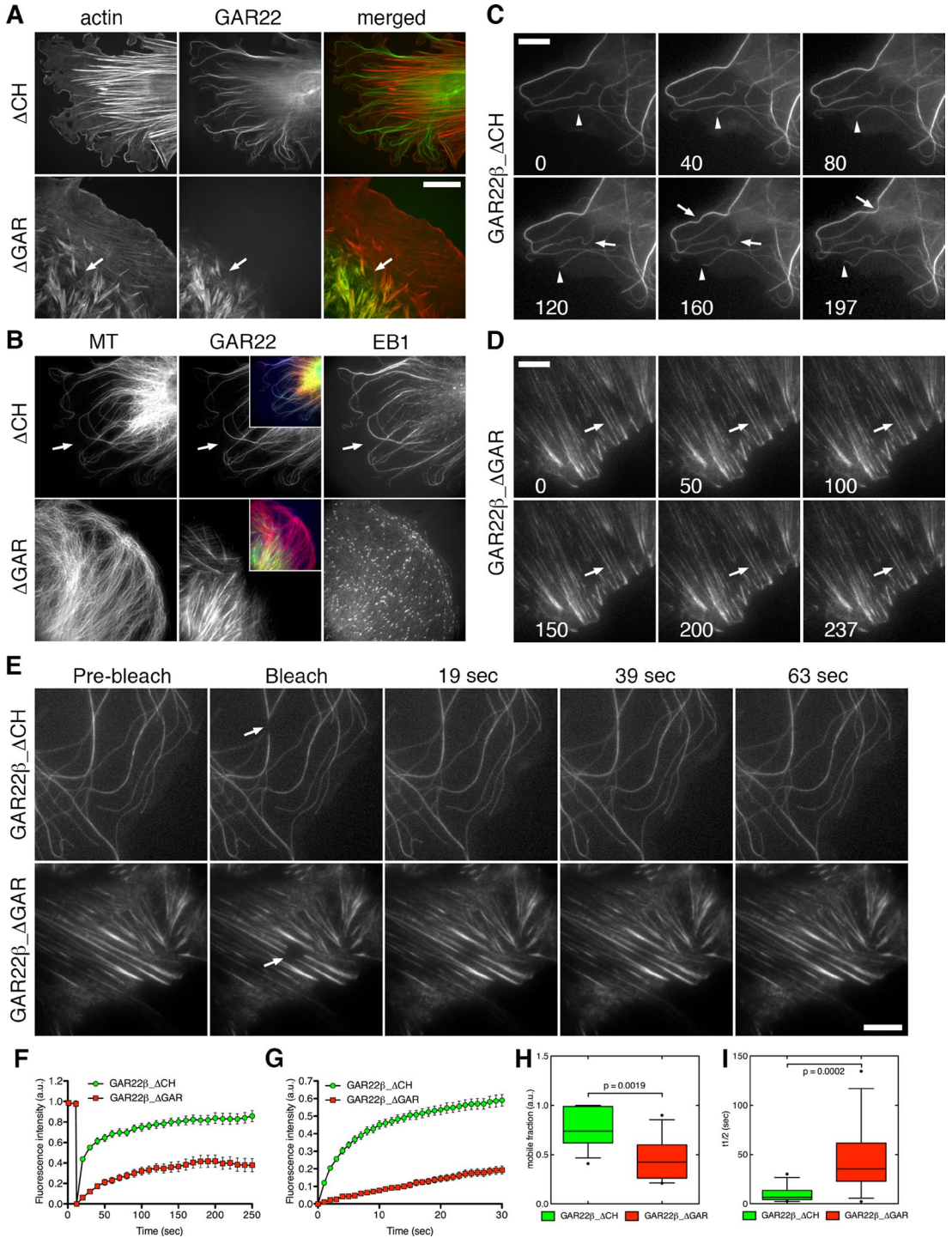

FIGURE 3: CH and GAR domains determine differential GAR22β localization and dynamics. (A, B) Sertoli cells expressing GAR22β_ΔCH or GAR22β_ΔGAR were fixed and stained with fluorescent phalloidin (A) or antibodies against tubulin and EB1 (B). GAR22β_ΔCH did not colocalize with the actin cytoskeleton (A), whereas GAR22β_ΔCH colocalized with thick MT bundles, which were robustly stained with EB1 (B, arrows). GAR22β_ΔGAR expression did not grossly affect the architecture of actin and MT cytoskeletons or EB1 localization at MT +tips. Of interest, GAR22β_ΔGAR colocalized with actin structures in the central cell region (A, arrows) but not with actin structures at the cell periphery. Scale bar, 5 μm. (C, D) Dynamics of GAR22β_ΔCH and GAR22β_ΔGAR. Expression of GAR22β_ΔCH in Sertoli cells caused the formation of thick MT bundles, which showed lateral fluctuations and buckling events (C, arrows). Arrowheads in C indicate one growing MT. GAR22β_ΔGAR dynamics at actin-like fibers was less prominent, resulting in very little GAR22β_ΔGAR turnover at these locations (D, arrows). Numbers indicate elapsed time in seconds. Scale bars, 10 μm. (E–I) FRAP analysis of GAR22β_ΔCH and GAR22β_ΔGAR kinetics in Sertoli cells. Areas associated with MT (for GAR22β_ΔCH) or actin (for GAR22β_ΔGAR) structures were bleached with a high intensity laser (arrows), and the subsequent recovery of the fluorescence signal was monitored over time (F, G). Note the faster kinetics of GAR22β_ΔCH, as indicated by its significantly higher mobile fraction (H) and lower half-time of recovery (I). Scale bar, 10 μm.

filaments, MTs, and EB1, we hypothesize that one potential function of GAR22β is to guide growing MTs along actin filaments. If our hypothesis is correct, then we expect to find EB1-positive MT ends moving along GAR22β-positive fibers (corresponding to actin filaments). We generated two populations of Sertoli cells in which GFP-tagged GAR22β was expressed at low or high levels. High levels of GAR22β caused EB1 mobilization to GAR22β-positive structures and its displacement from MT +tips, as well as bundling of MTs (Figure 5A, a–c). By contrast, in Sertoli cells expressing low levels of GAR22β, EB1 localization and MT architecture were not grossly altered. Moreover, we frequently observed EB1-positive MT ends in contact with GAR22β fibers and single MTs orientated parallel to and overlapping with GAR22β fibers (Figure 5A, d–f), as well as GAR22β-positive dots moving along GAR22β fibers (Supplemental Video8). To substantiate these observations, we transfected Sertoli cells with mCherry-tagged EB1 and visualized EB1 and GAR22β dynamics by TIRF microscopy. In cells expressing low GAR22β levels, we found that several EB1-positive MT growing ends moved along GAR22β fibers (Supplemental Video9). Thus these findings suggest that GAR22β guides growing MTs along actin filaments.

The novel noncanonical EB1-binding motif is crucial for the ability of GAR22β to regulate cell motility

Next we reasoned that if the interaction of GAR22β with EB1 via the novel noncanonical sequence is important for GAR22β function, then its deletion should abolish or reduce 1) its colocalization with and the displacement of EB1, 2) the bundling of the MT network, and 3) the regulation of cell motility.

We initially analyzed the subcellular localization of EB1 and MT architecture in Sertoli cells expressing high or low levels of GAR22β-ΔEBM. In cells expressing high levels of GAR22β-ΔEBM, the subcellular localization of EB1 was similar to that in control cells (Figure 5B, a–c, compared with Figure 5A, a–c), that is, EB1 was not often sequestered on GAR22β-positive fibers (arrowheads in Figure 5B, b and c). Moreover, regardless of the expression level of GAR22β-ΔEBM, the architecture of the MT network was not grossly altered (Figure 5Bd). Furthermore, Sertoli cells expressing the GAR22β-ΔEBM deletion mutant moved significantly faster than wild-type cells or cells expressing full-length GAR22β, and their motility was more similar to that of GAR22β$^{-/-}$ cells (Supplemental Figure 4D). Similarly, the overexpression of GAR22β-ΔEBM in NIH-3T3 cells impaired cell motility to a lower extent than full-length GAR22β (Supplemental Figure 4E). Furthermore, deletion of the noncanonical EB1-binding motif did not change the kinetics of GAR22β as determined by FRAP analysis (Figure 5, C–G, and Supplemental Fig5C_video11).

Thus these findings clearly indicate that the novel noncanonical EB1-binding sequence is crucial for GAR22β function.

Finally, we reasoned that if GAR22β–EB1 interaction were crucial for GAR22β function, then deletion of both EB1-binding motifs would completely abolish the phenotypic effect of GAR22β on EB1 subcellular distribution and cell motility. The double deletion mutant GAR22β-ΔEBMΔSxIP properly colocalized with microfilaments, indicating that the deletion of the two EB1-binding sites did not appreciably alter its interaction with actin (Figure 6A). As expected, in cells expressing high levels of GAR22β-ΔEBMΔSxIP, EB1 retained its localization at MT +tips and was not recruited to GAR22β-positive structures (Figure 6A compared with Figure 5, A and B). Moreover, the typical MT architecture was not altered in these cells (Figure 6A compared with Figure 5, A and B). Consistent with these observations, EB1 could not be immunoprecipitated from lysates of Sertoli cells expressing GAR22β-ΔEBMΔSxIP (Figure 6B). Furthermore, the motility of Sertoli cells expressing GAR22β-ΔEBMΔSxIP was not significantly different from that of GAR22β$^{-/-}$ cells (Figure 6C). Collectively these data clearly demonstrate that GAR22β–EB1 interaction is crucial for GAR22β function in the regulation of cell motility.

Deletion of GAR22β gene impairs spermatozoa motility and ultrastructure

Given the crucial role of GAR22β in the regulation of Sertoli cell motility and adhesion, we sought to analyze the consequences of *GAR22*β gene deletion on testis biology. In our GAR22β- knockout mouse, exons 3–6 and most of exon 7 were replaced with neomycin and LacZ cassettes, resulting in the complete loss of expression of GAR22β (and its splicing variant GAR22α; Figure 7, A and B). Spermatozoa generation in GAR22β$^{-/-}$ mice was significantly reduced ($(75.93 \pm 10.590) \times 10^6$/ml in WT [n = 9] and $(11.92 \pm 1.67) \times 10^6$/ml in GAR22β$^{-/-}$ [$n = 10$]; $p < 0.0001$), suggesting that GAR22β is involved in testicular physiology, spermatogenesis, and/or mature sperm function. Consistent with this hypothesis, we found that GAR22β is robustly expressed in adluminal parts of seminiferous tubules in adult mice (Figure 7C). However, because low levels of β-galactosidase expression can cause inconsistent X-Gal staining (Mahony *et al.*, 2002), we cannot exclude GAR22β expression in premeiotic germ or Sertoli cells. Of interest, GAR22β expression was not detectable in seminiferous tubules of juvenile (up to 7 d old) mice (Figure 7C). At this developmental stage, seminiferous tubules consist exclusively of immature, highly proliferative Sertoli cells and type A spermatogonia (Bellve *et al.*, 1977; Veitinger *et al.*, 2011), suggesting that substantial GAR22β expression coincides with germ cells entering meiotic and/or postmeiotic stages of the seminiferous cycle. At the subcellular level, we found substantial GAR22β colocalization with the actin cytoskeleton. In wild-type seminiferous tubules, spatial overlap was most pronounced at the adluminal Sertoli junctions and apical ectoplasmic specializations (Figure 7D). By contrast, no such signals were observed in seminiferous tubules from GAR22β$^{-/-}$ mice (Supplemental Figure S6).

Given the robust expression of GAR22β in seminiferous tubules' adluminal compartment—the site of spermiogenesis and spermiation—we hypothesized that GAR22β expression could play a morphological and/or functional role in sperm biology. Spermatozoa isolated from epididymides of wild-type mice have a typical elongated shape and a curved head. In wild-type spermatozoa, GAR22β is detectable at the head and along the entire length of the flagellum (Figure 8A). By contrast, GAR22β was absent in GAR22β$^{-/-}$ spermatozoa (Figure 8A), which often displayed flagellar angulation at approximately the junction of the midpiece with the principal piece leading to hairpin-bend morphology (Figures 8A and 9B). This morphological defect has been shown to correlate with mouse infertility (Yeung *et al.*, 1999), further supporting our hypothesis that GAR22β is involved in testicular physiology.

We also found that the percentage of motile spermatozoa and their velocity and head oscillations (lateral amplitude) were all significantly reduced in GAR22β$^{-/-}$ mice (Figure 8, B–G). Consistent with impaired spermatozoa motility, the typical axoneme ultrastructure was also altered in GAR22β$^{-/-}$ mice, as characterized by missing or misplaced microtubule doublets and outer dense fibers (Figure 9, C–H; spermatozoa with normal axoneme: WT [$n = 183$], 86.3 ± 3.9%; GAR22β$^{-/-}$ ($n = 186$), 48.4 ± 0.1%; spermatozoa with crippled axoneme: WT, 13.7 ± 3.9%; GAR22β$^{-/-}$, 51.6 ± 0.1%). Of note, these phenotypic alterations were concomitant with a strong decrease in F-actin expression in seminiferous tubules (Figure 10). Although not resulting in the loss of intercellular adhesions, F-actin reduction was most pronounced at the basal membrane and the

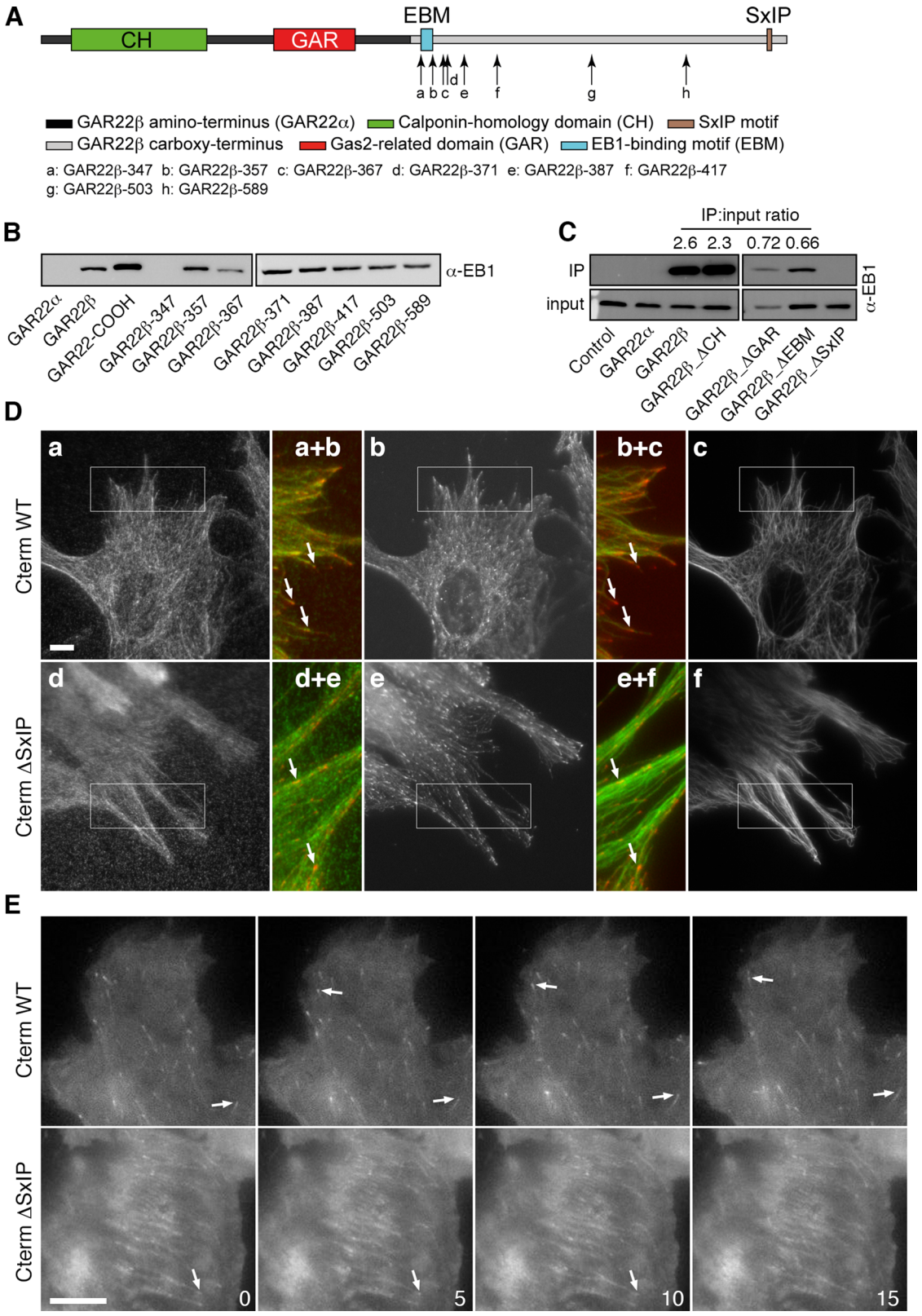

FIGURE 4: GAR22β directly interacts with EB1 via a novel noncanonical motif. (A) Schematics of GAR22β protein structure and its deletion mutants used in this study. (B, C) In vitro binding assay between purified EB1 and GAR22β deletion mutants, showing the presence of a noncanonical EB1-binding motif between amino acids 347 and 357. (C) Analysis of GAR22β-EB1 interaction in vivo. Lysates of untransfected cells and cells expressing some GAR22β deletion mutants were immunoprecipitated with anti-GFP antibodies and probed with anti-EB1 antibodies. GAR22α served as negative control (no EB1 binding). Control lane indicates unprocessed cell lysate (no immunoprecipitate [IP]). Deletion of the CH domain had no effect on the ability of GAR22β to interact with EB1. Conversely, deletion of either

luminal ectoplasmic specialization (ES) surrounding elongated spermatids (Figure 10). Together these results suggest that GAR22β is critically involved in proper spermatid elongation and axoneme development.

DISCUSSION

In the present study, we identified a novel noncanonical EB1-binding motif within the C-terminal portion of GAR22β. We also demonstrated that GAR22β regulates lamellipodia dynamics, FA turnover, and directional cell motility. Using a GAR22β-knockout mouse, we demonstrated that these mice generate fewer and severely impaired spermatozoa characterized by crippled motility as well as axoneme ultrastructure. Our findings provide novel insights into the function of GAR22β that could be instructive for understanding how proteins of this family coordinate the functions of the actin and MT cytoskeletons during cell motility and other cytoskeleton-dependent processes.

Our data clearly suggest that GAR22β regulates cell motility through the modulation of FA turnover and lamellipodia activity. GAR22β deficiency caused an increase of both FA assembly and disassembly rates. Given the impaired motility and increased FA stability in cells expressing high levels of GAR22β, the faster motile phenotype of GAR22β$^{-/-}$ cells could be due to decreased FA stability or density. This possibility is consistent with the observation that vinculin$^{-/-}$ cells move faster and have a reduced FA density than wild-type cells (Mierke *et al.*, 2010). Moreover, given that MTs affect FA dynamics by promoting FA dissociation (Kaverina *et al.*, 1999; Ballestrem *et al.*, 2000; Krylyshkina *et al.*, 2002), it is conceivable that GAR22β influences FA turnover via its stabilizing effect on MTs.

Increased GAR22β expression also caused impairment of lamellipodia activity and MT dynamics and redistribution of EB1 along the entire MT network. In this context, it has been shown that disruption of MTs or reduction of MT dynamics impairs lamellipodia formation and that MT growth locally drives lamellipodia protrusion by delivery of active Rac 1 (Vasiliev *et al.*, 1970; Goldman, 1971; Bershadsky *et al.*, 1991; Liao *et al.*, 1995; Dunn *et al.*, 1997; Mikhailov *et al.*, 1998; Waterman-Storer *et al.*, 1999). Furthermore, EB1 overexpression causes MT bundling (Bu and Su, 2001; Ligon *et al.*, 2003), whereas its down-regulation inhibits both MT stabilization and cell migration (Wen *et al.*, 2004; Schober *et al.*, 2009; Pfister *et al.*, 2012). EB1 overexpression also causes the displacement of WAVE2, a key regulator of directional cell motility (Yamazaki *et al.*, 2003), from protruding lamellipodia (Schober *et al.*, 2012). Hence GAR22β likely regulates cell migration through its dual interaction with EB1 and MTs.

Of note, we observed both the colocalization of GAR22β with dynamic MTs and the movement of EB1-positive MT tips along GAR22β fiber-like structures (corresponding to actin fibers). This observations support a role for GAR22β in MT movement along polarized actin fibers similar to other actin- and MT-binding proteins (Rodriguez *et al.*, 2003). Collectively our findings are thus consistent with a mechanism by which cell motility is regulated by GAR22β-mediated control of FA turnover, EB1 subcellular localization, and MT dynamics.

All known EB1-binding proteins harbor the classical SxIP EB1-binding motif, and their recruitment to MT growing tips is exclusively mediated by EB1 (Honnappa *et al.*, 2009). We showed here that GAR22β interacts with EB1 not only via the SxIP motif, but also through a novel noncanonical motif located at the beginning of its C-terminal portion. Furthermore, deletion of the noncanonical EB1-binding motif not only decreases the interaction of GAR22β with EB1 and the displacement of EB1 from MT +tips, but it also impairs the ability of GAR22β to regulate cell motility, suggesting that it is important for GAR22β function. As to the structural basis of the interaction(s) between the noncanonical EB1-binding motif of GAR22β and the EB1 dimer, the lack of information on GAR22β protein folding makes it difficult to put forward any precise hypothesis. We note, however, that sequences in adenomatous polyposis coli, MACF, and Short Stop are characterized by conserved serines and positively charged amino acids that interact with the C-terminal portion of EB1 (Slep *et al.*, 2005). Because the novel noncanonical EB1-binding motif of GAR22β also contains conserved serines and positively charged amino acids, we speculate that the noncanonical EB1-binding motif of GAR22β interacts with EB1 in a similar way. Moreover, the C-terminal sequence of GAR22β exhibits a highly disordered and flexible structure, as predicted by secondary structure prediction tools. Therefore it is conceivable that the two EB1-binding sites of GAR22β could be juxtaposed to achieve optimal interaction with EB1 dimers. Future crystallographic studies will provide a clear picture of the structural determinants of GAR22β-EB1 interaction(s).

As to the functions of CH and GAR domains, we demonstrated that both are required for GAR22β's ability to regulate cell motility. In the absence of the CH domain, the binding properties of the GAR domain predominate to cause both MT bundling and severe impairment of MT dynamics, likely arising by the delocalization of EB1 from MT +ends. The deletion of the GAR domain of GAR22β promotes a milder phenotype, in that MT dynamics is not grossly affected, and EB1 primarily localizes to MT +tips. Remarkably, GAR22β-ΔGAR localizes to only a subset of actin-rich structures, suggesting that the GAR domain could support differential interactions of GAR22β with the actin cytoskeleton. Also note that the interaction of GAR22β with actin is stronger than its interaction with MTs, as indicated by lower kinetics of GAR22β-ΔGAR, thus explaining the

the GAR domain or the noncanonical EB1-binding motif reduced the amount of EB1 in GAR22β IPs. Deletion of the SxIP resulted in undetectable GAR22β–EB1 interaction. IP:input ratios were calculated from densitometry scans by dividing the intensity of EB1 bands in the IPs by the intensity of the corresponding EB1 bands in the inputs. (D) The novel noncanonical EB1-binding motif is sufficient for localization of the GAR22β C-terminal (Cterm) portion to MT +tips. Sertoli cells expressing GAR22β Cterm (a) or Cterm ΔSxIP (d) were fixed and stained with antibodies against EB1 (b, e) and tubulin (c, f). Colored images show enlarged views of the boxed areas in a–f. In the colored images MTs and GAR22β Cterm(s) are shown in green, and EB1 is shown in red. Consistent with in vitro binding assays, GAR22β Cterm (a) colocalized with EB1 (b) at MT +tips (c; see arrows in a+b and b+c). Despite the deletion of the canonical SxIP motif (GAR22β Cterm ΔSxIP), GAR22β Cterm (d) still colocalizes with EB1 (e) at MT tips (f; see arrows in d+e and e+f), indicating that the novel noncanonical EB1-binding motif is sufficient for mediating GAR22β-EB1 interaction. Scale bar, 10 μm. (E) Dynamics of GAR22β Cterm and Cterm ΔSxIP. Sertoli cells expressing GFP-tagged GAR22β Cterm or GAR22β Cterm ΔSxIP were imaged using TIRF microscopy. Note the localization of both GAR22β Cterm and GAR22β Cterm ΔSxIP at MT +tips (arrows; the dynamics of GAR22β Cterm ΔSxIP can be better appreciated in Supplemental Fig4E_video10). Numbers indicate elapsed time in seconds. Scale bar, 10 μm.

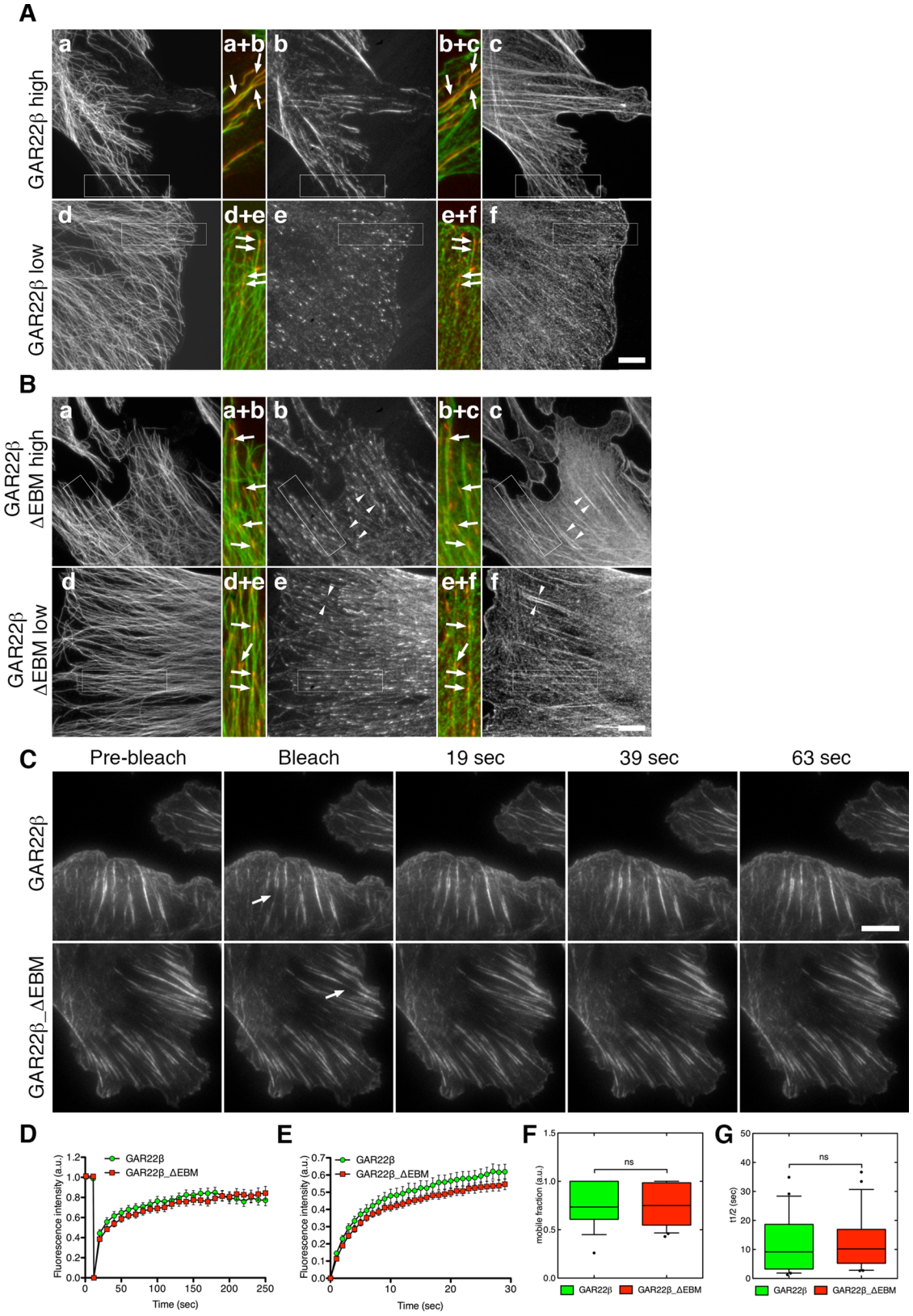

FIGURE 5: Influence of GAR22β expression levels on MT architecture and EB1 localization. (A) Sertoli cells expressing high or low levels of GFP-GAR22β were fixed and labeled with anti-tubulin (a, d) and anti-EB1 (b, e) antibodies. Colored images show enlarged views of the boxed areas in a–f. In Sertoli cells expressing high levels of GAR22β, EB1 was displaced from its normal subcellular localization (at MT +tips; see Figure 1) and accumulated on GAR22β-positive structures (b, c; arrows in b+c; GAR22β, green; EB1, red). Under these conditions, the architecture of MT cytoskeleton was also altered, resulting in the bundling of single MTs (arrows in a+b; MT, green; EB1, red). By contrast, the expression of low levels of full-length GAR22β did not grossly affect MT architecture or EB1 localization

predominant localization of full-length GAR22β to the actin cytoskeleton. We speculate that the preferential localization of GAR22β to actin fibers is important for its ability to guide growing MTs along actin filaments.

As to the role of GAR22β in testicular physiology, it is known that specialized junctions between adjacent Sertoli cells—the apical ES and the blood–testis barrier (BTB), which are both enriched with cytoskeletal components—play crucial roles in supporting germ cell differentiation and movement across the seminiferous epithelium until spermatids are released in the tubule lumen at spermiation (Lie *et al*. 2010a). It has been appreciated that actin and MT cytoskeletons are essential for spermatogenesis. Disruption of MTs causes abnormal germ cell positioning, detachment, and apoptosis. MTs are required for spermatid movement (O'Donnell and O'Brian, 2014), and deletion of α-tubulin acetyltransferase causes reduction of mouse male fertility and sperm motility, as well as higher MT stability (Kalebic *et al*., 2013). Because GAR22β$^{-/-}$ mice are also characterized by reduction of male fertility and sperm motility, it is conceivable that GAR22β regulates MT function during the different spermatogenesis stages, possibly via its dual interaction with MTs and EB1. Of interest, microtubule-based motor proteins localize at the apical ES (Vaid *et al.*, 2007). Moreover, we showed that GAR22β colocalizes with actin at Sertoli junctions and apical ES. Hence we speculate that GAR22β could be involved in MT-based vesicle transport during restructuring of apical ES, for example, through its ability to guide MTs along actin filaments. Many studies have shown that several actin cytoskeleton–associated proteins localize at the apical ES and BTB and that their expression spatially and temporally correlates with the restructuring of the apical ES and BTB (Lie *et al.*, 2009, 2010b; Young *et al.*, 2009; Wong *et al.*, 2010; Li *et al.*, 2011; Su *et al.*, 2012; Qian *et al.*, 2013, 2014; Gungor-Ordueri *et al.*, 2014). Of importance, pharmaceutical inhibition, or down-regulation, of some actin cytoskeleton–associated proteins alters Sertoli cell tight junction permeability, perturbs restructuring of the apical ES and BTB, and blocks spermatid transport, causing defects in sperm release (Lie *et al.*, 2010b; Qian *et al.*, 2013; Gungor-Ordueri *et al.*, 2014). In this context, our findings show that F-actin levels are reduced in GAR22β$^{-/-}$ testes and that sperm production is reduced in GAR22β$^{-/-}$ mice suggesting that GAR22β regulates actin remodeling required for efficient spermatogenesis.

Collectively our findings demonstrated that GAR22β plays a crucial role in the regulation of cell migration and adhesion and spermatozoa motility and ultrastructure. Several questions remain to be addressed. For instance, how does GAR22β regulate spermatogenesis? At which stages is it expressed? How is GAR22β involved in the restructuring of the apical ES and BTB? How does it regulate the functional interplay between actin and MTs? The answers to these questions will help to better understand not only the function(s) of GAR22β (and similar proteins), but also the regulation of the molecular mechanisms underlying cell motility and spermatogenesis.

MATERIALS AND METHODS

Cell culture

NIH-3T3 (American Type Culture Collection (ATCC), Manassas, VA; CRL 1658), B16F1 (ATCC CRL 6323), and the packaging cells Phoenix-Ampho (ATCC SD 3443) and Phoenix-Eco (ATCC SD 3444) were grown in DMEM high glucose supplemented with 10% fetal calf serum (FCS), 2 mM L-glutamine, 1 mM sodium pyruvate, 100 µg/ml streptomycin, and 100 U/ml penicillin. All cell lines were grown at 37°C/5% CO_2.

Generation of GAR22β-knockout mice and Sertoli cell lines

GAR22β-knockout mice were generated according to standard protocols at the Institut für Versuchstierkunde (Uniklinik RWTH Aachen, Aachen, Germany) using ES cells (clone CH10) purchased from the Knockout Mouse Project (University of California, Davis, Davis, CA) in which the *GAR22β* gene was replaced with a selection marker and a LacZ cassette.

For the generation of Sertoli cell lines, testes from 2- to 3-wk-old mice were explanted and placed in phosphate-buffered saline (PBS) containing 100 IU/ml penicillin and 100 µg/ml streptomycin. After two washes with PBS, the tunica albuginea was removed, and the seminiferous tubules (STs) were cut into pieces and digested with 0.5 mg/ml collagenase IA until the STs become well separated. The STs were then dispersed by pipetting several times, and the resulting fragments were centrifuged at 200 × *g* for 5 min at room temperature. After washing of the pellet (containing ST fragments) twice with PBS, STs were incubated with 0.25% trypsin/EDTA solution for 5 min at 37°C. Trypsin action was terminated when STs became completely digested by adding 20% fetal bovine serum. Digested STs were filtered through a 40-µm cell strainer and centrifuged at 500 × *g* for 4 min at room temperature. At this stage, the pellet primarily contained Sertoli cells, which were washed once with PBS and four times with Sertoli cell growth medium (DMEM/F12 [1:1], 10% FCS, 2 mM L-glutamine, 100 IU/ml penicillin, and 100 µg/ml streptomycin). Sertoli cells were grown at 37°C/5% CO_2. Within the first 24 h after seeding, residual nonadherent cells were removed by washing several times with growth medium. Sertoli cells were immortalized by infecting them with dominant-negative p53 (kindly provided by Andrei Gudkov, Roswell Park Cancer Institute, Buffalo, NY; Ossovskaya *et al*., 1996) using ecotropic retroviruses (see later discussion). To generate Sertoli cell lines expressing GFP-GAR22β

(d–f; arrows in d+e; MT, green; EB1, red). In these cells, EB1-positive MT +tips were often associated with GAR22β-positive fibers (arrows in e+f; GAR22β, green; EB1, red) with single MTs running parallel to GAR22β-positive fibers (arrows in d+e; MT, green; EB1, red). Scale bar, 10 µm. (B) Deletion of the noncanonical EB1-binding motif of GAR22β significantly reduces both GAR22β-EB1 colocalization and GAR22β influence on MT architecture. Sertoli cells expressing high or low levels of GFP-GAR22β-ΔEBM were fixed and labeled with anti-tubulin (a, d) and anti-EB1 (b, e) antibodies. Colored images show enlarged views of the boxed areas in a–f. Sertoli cells expressing high levels of GAR22β-ΔEBM showed normal MT structure (a) and reduced accumulation of EB1 at GAR22β-positive fibers (arrowheads in b+c). In these cells, EB1 tips were often associated along GAR22β-positive fibers (arrows in b+c; GAR22β, green; EB1, red). The expression of low levels of GAR22β-ΔEBM did not cause obvious phenotypic alterations, resulting in normal EB1 localization to MT tips (arrows in d+e; MT, green; EB1, red). EB1 tips were often also associated along GAR22β-positive fibers (arrowheads in e+f; see arrows in e and f; GAR22β, green; EB1, red). Scale bar, 10 µm. (C–G) Deletion of the noncanonical EB1-binding motif does not affect the turnover of GAR22β kinetics. FRAP analysis of GAR22β and GAR22β_ΔEBM kinetics in Sertoli cells. Similar areas (arrows) in cells expressing GAR22β or GAR22β_ΔEBM were bleached with a high-intensity laser (arrows), and the subsequent recovery of the fluorescence signal was monitored over time (D–G). Note the similar kinetics of GAR22β and GAR22β_ΔEBM, as indicated by comparable mobile fraction (F) and half-time of recovery (G). Scale bar, 10 µm.

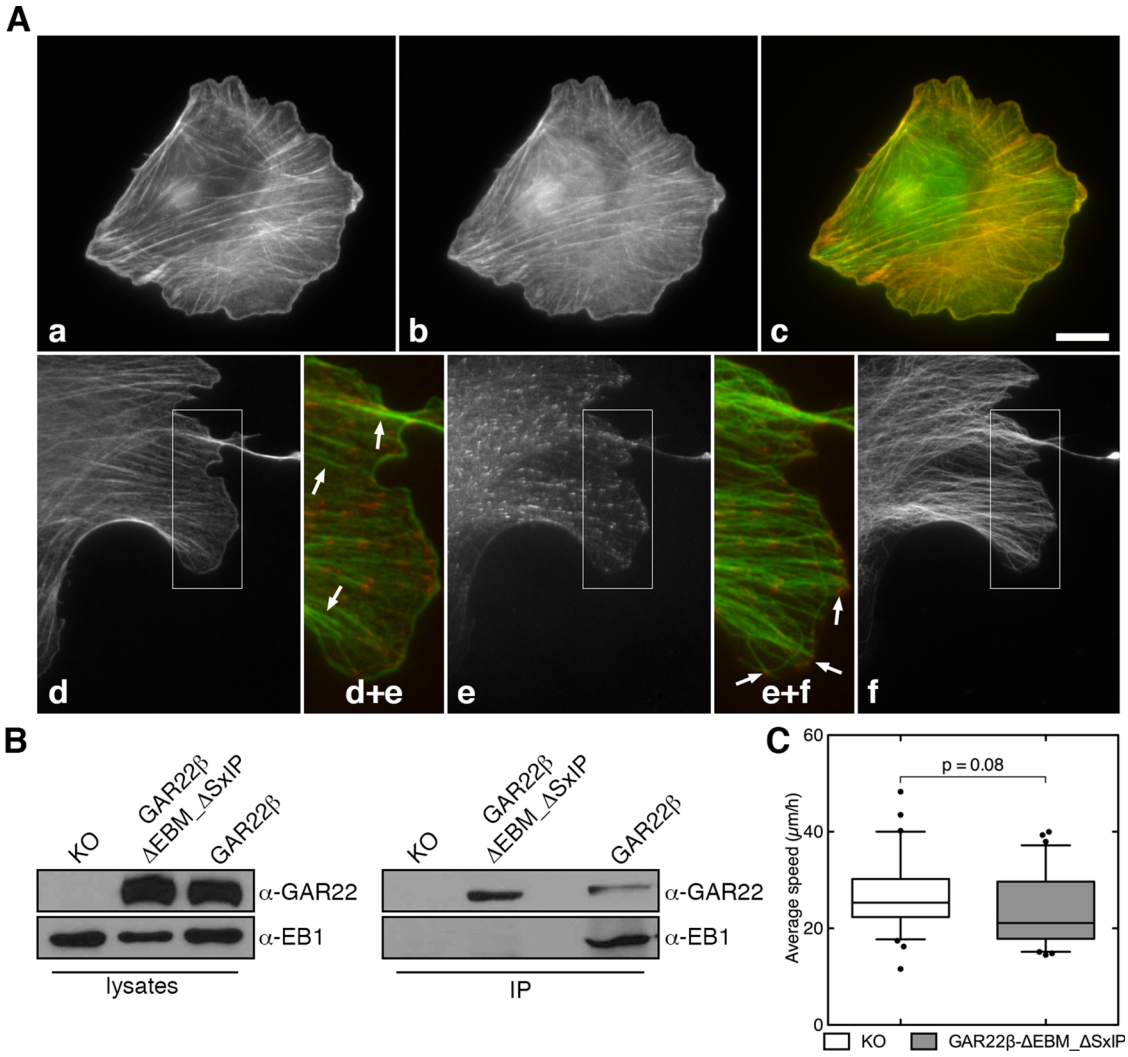

FIGURE 6: Deletion of both EB1-binding sites of GAR22β abolishes its ability to both displace EB1 from its subcellular localization and regulate cell motility. (A) Deletion of both EB1-binding sites of GAR22β abolishes its ability to displace EB1 from its normal subcellular localization. Sertoli cells expressing GFP-tagged GAR22β-ΔEBMΔSxIP (b, d) were fixed and stained with fluorescent phalloidin (a) and antibodies against EB1 (e) and tubulin (f). Note the substantial colocalization of GAR22β-ΔEBMΔSxIP with actin cytoskeleton (c; GAR22β-ΔEBMΔSxIP is shown in green, and actin is shown in red), indicating that the deletion of the two EB1-binding sites did not grossly alter its interaction with actin. Remarkably, the expression of GAR22β-ΔEBMΔSxIP did not cause EB1 recruitment at GAR22β-ΔEBMΔSxIP-positive structures or alter MT architecture (arrows in d+e; compare with Figure 5, A and B). In these cells, EB1 retained its typical localization at MT +tips (arrows in e+f). Colored images show enlarged views of the boxed areas in d–f. In the colored images. MTs and GAR22β-ΔEBMΔSxIP are shown in green and EB1 is shown in red. Scale bar, 10 μm. (B) Analysis of the interaction between GAR22β-ΔEBMΔSxIP and EB1. Lysates of GAR22β$^{-/-}$ Sertoli cells and GAR22β$^{-/-}$ Sertoli cells expressing GAR22β-ΔEBMΔSxIP or full length GAR22β were immunoprecipitated with anti-GFP antibodies and probed with anti-EB1 antibodies. GAR22β$^{-/-}$ Sertoli cells served as negative control (no EB1 binding). Deletion of both EB1-binding motifs completely abolished the ability of GAR22β to interact with EB1, which was present only in lysates of Sertoli cells expressing full-length GAR22β. Lysates show the expression of GAR22β and EB1. (C) Analysis of Sertoli cell motility, showing that the motility of cells expressing GAR22β-ΔEBMΔSxIP did not significantly differ from that of GAR22β$^{-/-}$ cells. Graph shows average speed values as determined from wound-healing assays. In the box-and-whisker plots, the line in the middle of the box indicates the median, the top of the box indicates the 75th quartile, and the bottom of the box indicates the 25th quartile. Whiskers represent the 10th (lower) and 90th (upper) percentiles.

or GAR22β deletion mutants, cells were infected with pMSCV-based ecotropic retroviruses. Cell populations expressing high or low GFP levels were sorted by fluorescence-activated cell sorting. For the analysis of MT dynamics, Sertoli cells were infected with ecotropic retroviruses carrying a pMSCV-based mCherry-EB1 construct.

Plasmid generation, protein production and purification, in vitro binding assays, and immunoprecipitation

The generation of the plasmids, protein production and purification, and in vitro binding assays and immunoprecipitation are described in Supplemental Table S1 and Supplemental Materials and Methods.

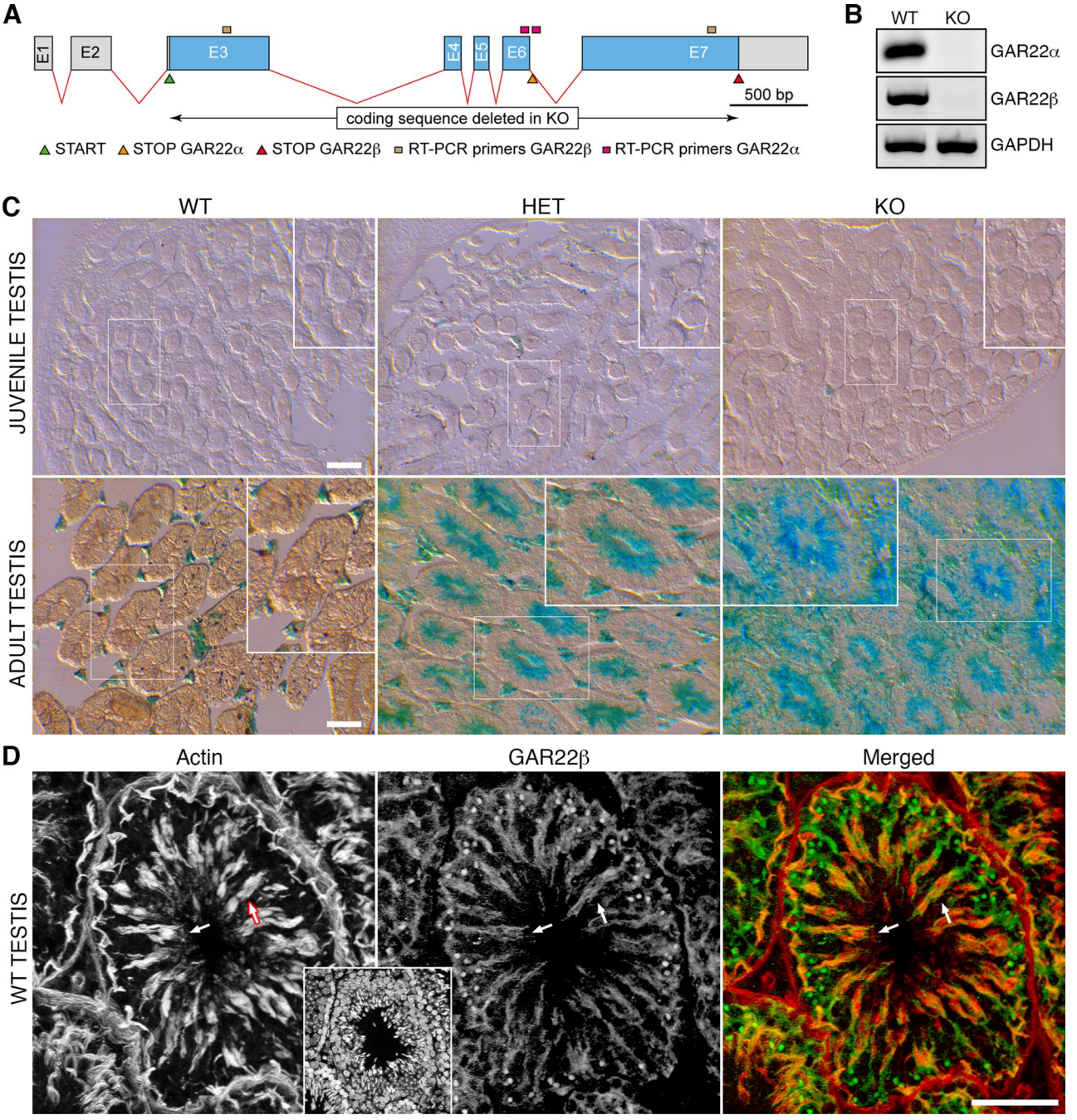

FIGURE 7: GAR22β is expressed in seminiferous tubuli of adult but not juvenile mice. (A) Schematics of exon–intron structure of the GAR22β gene. (B) RT-PCR analysis of GAR22α and GAR22β expression in Sertoli cells isolated from wild-type or GAR22β$^{-/-}$ testes. GAPDH served as loading control. (C) Expression of GAR22β in juvenile and adult seminiferous tubuli. Cryosections of WT, heterozygote (HET), and GAR22β$^{-/-}$ (KO) testes were stained with X-Gal solution. GAR22β was primarily expressed in adluminal regions of seminiferous tubuli. Thin-lined boxes indicate the area enlarged in the thicker-lined boxes. Scale bars, 100 μm. (D) GAR22β colocalizes with actin in seminiferous tubules. Cryosections of wild-type testes were stained with fluorescent phalloidin, GAR22β antibodies, and DAPI and then analyzed by confocal microscopy. Actin was distributed throughout the seminiferous tubuli, where it colocalized at many locations with GAR22β (arrows). In the merged image, actin is shown in red and GAR22β in green. Inset shows DAPI staining. Scale bar, 50 μm.

Transfection

Transient gene expression was obtained after transfection by standard calcium phosphate precipitation. Stable gene expression was obtained by viral-mediated gene delivery. Briefly, the pMSCV-based constructs were cotransfected with the pVPack-GP vector (carrying the gag and pol viral genes) and with pVPack-Eco (carrying the envelope viral gene) into Phoenix packaging cells by using a calcium phosphate transfection procedure. Two days later, the cell medium containing the retroviral particles was collected and used to infect the target cells. Infected cells were selected with puromycin (1–4 μg/ml, depending on the cell type) for 2 wk.

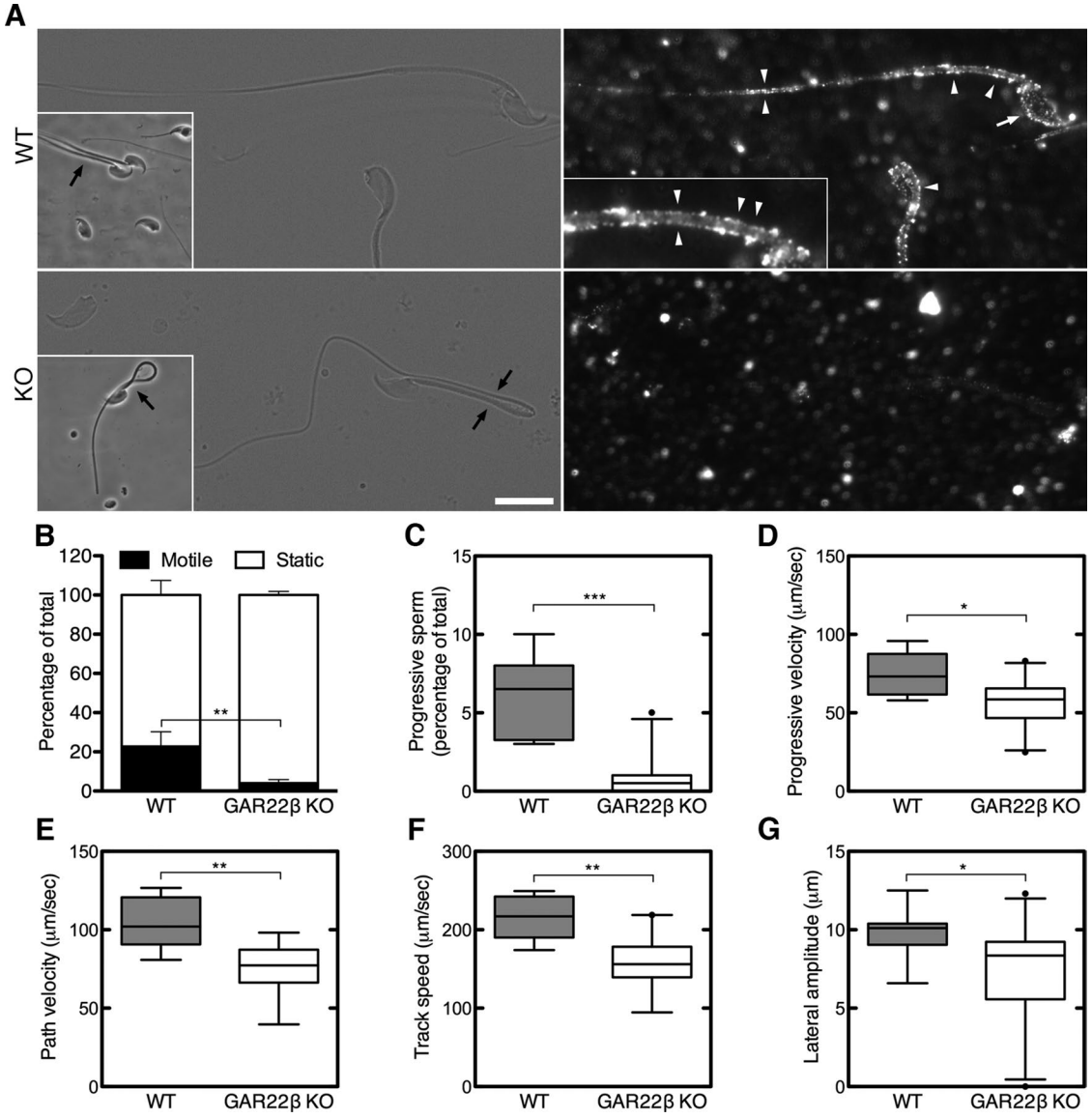

FIGURE 8: GAR22β localizes at the head and flagellum of mouse spermatozoa and is essential for their efficient motility. (A) Localization of GAR22β in mouse spermatozoa. Epididymal spermatozoa from wild-type and GAR22β$^{-/-}$ mice were plated on glass coverslips, fixed, and stained with antibodies against GAR22β. GAR22β localized at the head and along the entire flagellum of wild-type spermatozoa, which have a typical elongated morphology. GAR22β is not detectable along GAR22β$^{-/-}$ spermatozoa, which had an altered morphology, characterized by an 180° bend at approximately the end of the midpiece (arrows), causing spermatozoa to fold onto themselves. Scale bar, 10 μm. (B–G) Box-and-whiskers plots, showing the analysis of spermatozoa motility. Note the significant decrease in number of motile spermatozoa (B), spermatozoa velocity (C–F), and head lateral amplitude (G) in GAR22β$^{-/-}$mice. $p = 0.0015$ (**, B), 0.0010 (***, C), 0.02 (*, D), 0.002 (**, E, F), 0.04 (*, G).

Immunofluorescence microscopy

Cells were fixed with 4% paraformaldehyde in cytoskeleton buffer (10 mM 1,4-piperazinediethanesulfonic acid, 150 mM NaCl, 5 mM ethylene glycol tetraacetic acid, 5 mM glucose, and 5 mM $MgCl_2$, pH 7.0) for 20 min at room temperature and then extracted with 0.1% Triton X-100 in cytoskeleton buffer for 2 min at room temperature. For EB1 and tubulin labeling, cells were fixed with ice-cold (–20°C) methanol for 4 min, rehydrated with Tris-buffered saline (TBS) containing 0.1% Triton X-100 (3 × 5 min), and finally washed with TBS. Immunofluorescence labeling was done using Alexa 594– or Alexa 350–conjugated phalloidin (Life Technologies, Carlsbad, CA) and antibodies against EB1 (clone 5; BD Transduction Laboratories, Heidelberg, Germany), tubulin (hybridoma supernatant; clone YL1/2), and GAR22β (Gamper *et al*. 2009). Secondary antibodies were Alexa 594 anti-mouse immunoglobulin G (IgG) and Alexa 594 and Alexa 350 anti-rat IgG (all from Life Technologies). Coverslips were mounted in Prolong Gold antifade agent (Life Technologies). For immunofluorescence microscopy of mouse testes, cryosections were labeled with Alexa 555–conjugated phalloidin (Life Technologies), 4′,6-diamidino-2-phenylindole (DAPI) and GAR22β antibody (in combination with Alexa 488 anti-rabbit IgG). Images were taken using an upright fixed-stage scanning confocal microscope (Leica TCS SP5 DM6000 CFS; Leica Microsystems, Wetzlar, Germany)

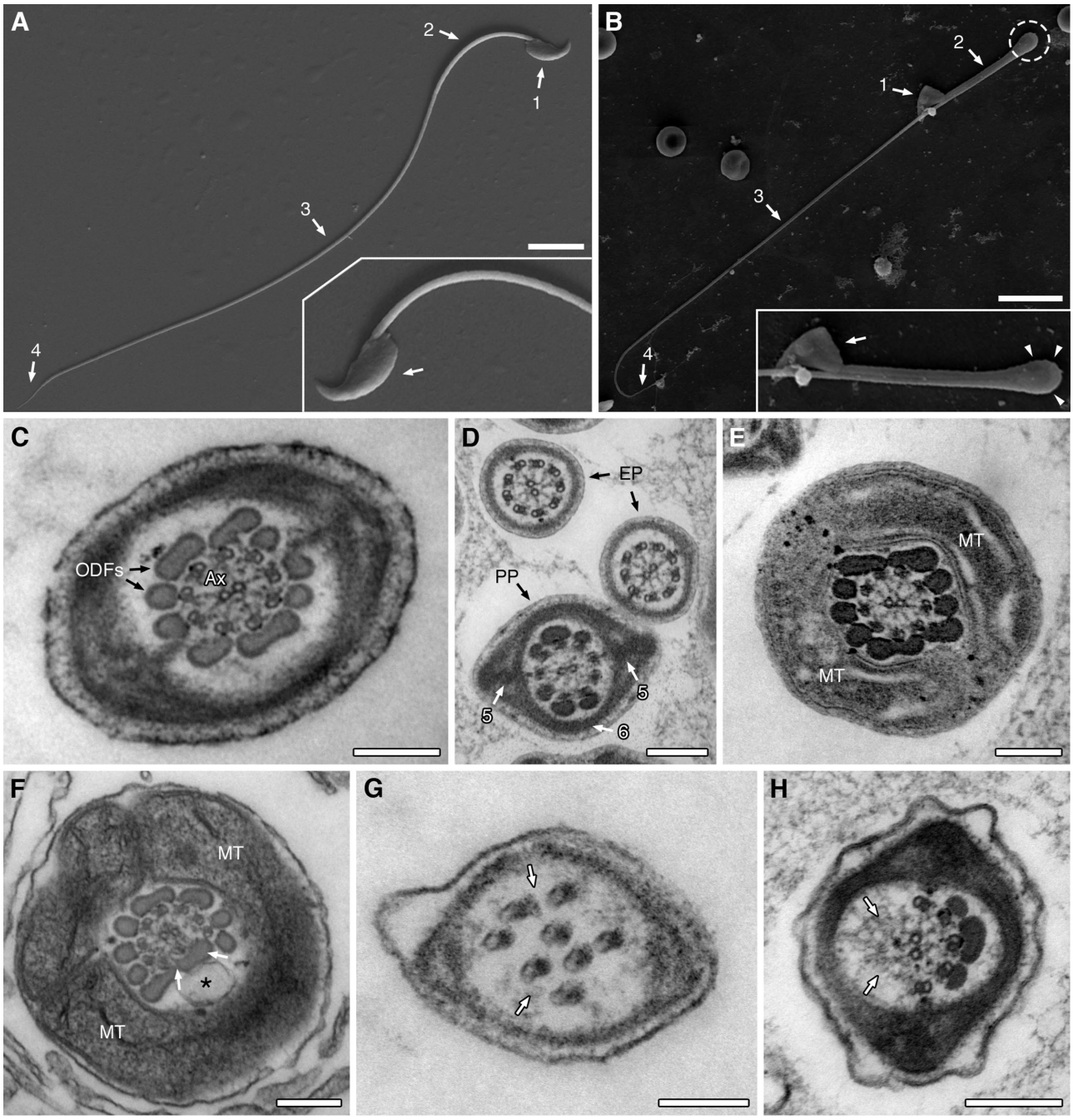

FIGURE 9: Lack of GAR22β induces abnormalities of spermatozoa morphology and axoneme ultrastructure in mouse spermatozoa. (A, B) Scanning electron microscopy analysis of wild-type (A) and GAR22β$^{-/-}$ spermatozoa (B). Wild-type spermatozoa were characterized by a falciform-shaped head (1) and slightly undulated mid piece (2) and tail (3, 4). Conversely, GAR22β$^{-/-}$ spermatozoa showed altered head morphology (arrows) and a prominent 180° bend at approximately the end of the midpiece (dashed circle and arrowheads in inset). Scale bars, 10 μm (5 μm for insets). (C–H) Transmission electron microscopy analysis of wild-type (C–E) and GAR22β$^{-/-}$ (F–H) spermatozoa. Cross sections at different locations along wild-type spermatozoa showed normal axoneme structure (C; Ax) characterized by the classical 9+2 microtubule doublet arrangement (C–E). Also shown are typical structure and distribution of outer dense fibers (ODFs), longitudinal columns of the fibrous sheath (5), circumferential ribs of the fibrous sheath (6), and mitochondria. EP, end piece; PP, principal piece. By contrast, the ultrastructure of GAR22β$^{-/-}$ spermatozoa was severely altered, as indicated by the presence of axonemes with missing (arrows in G, H) or misplaced microtubule doublets and outer dense fibers (arrows in F). Asterisk in F indicates a large, vesicle-like structure displacing one ODF from its normal location. Scale bars, 200 nm.

equipped with a 20×/1.0 numerical aperture water immersion objective (HCX APO L; Leica Microsystems). To control for nonspecific staining, experiments in which the primary antibodies were omitted were performed in parallel with each procedure. Digital images were uniformly adjusted for brightness and contrast using Imaris 8.1 software (Bitplane, Zurich, Switzerland).

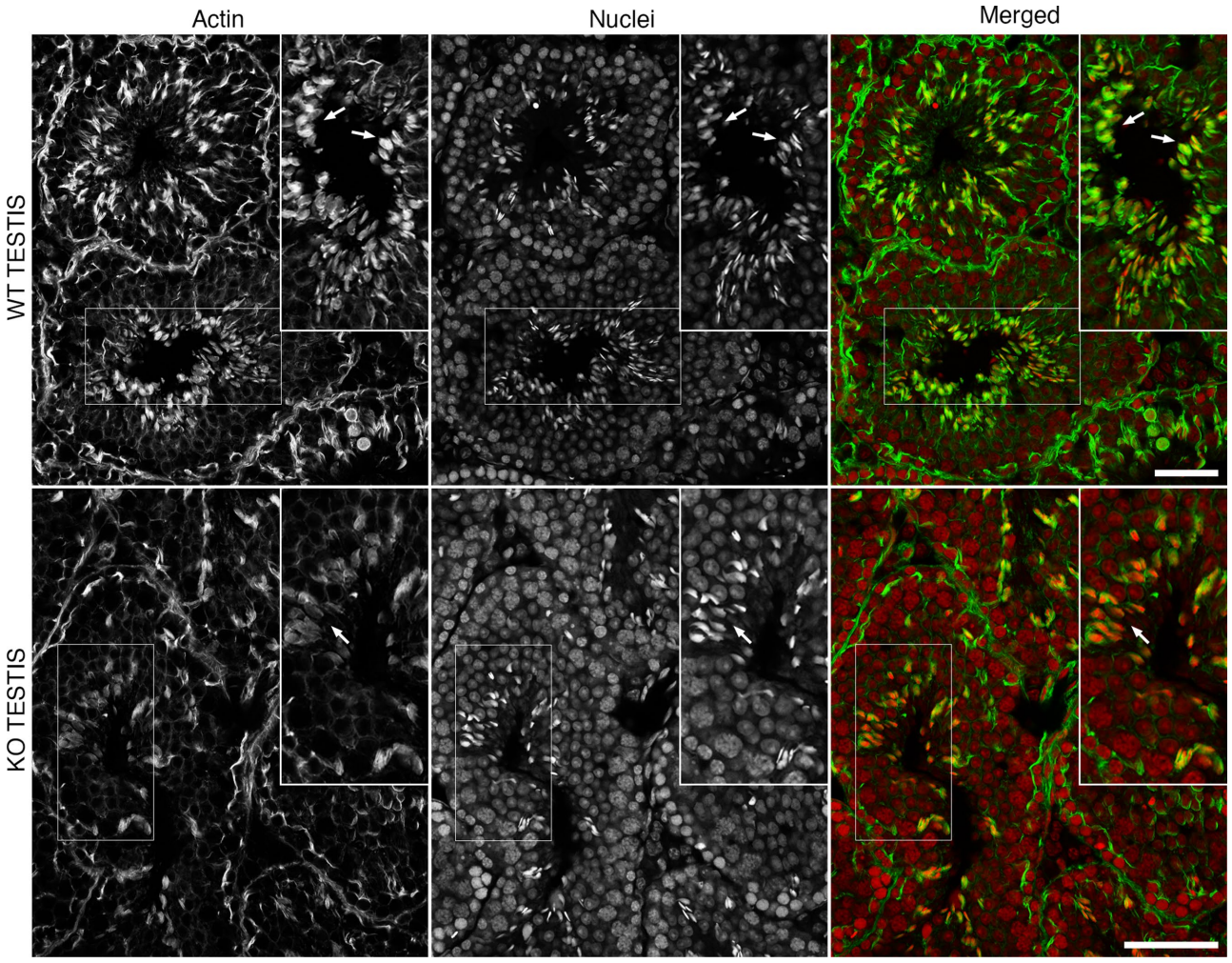

FIGURE 10: Deletion of GAR22β causes severe reduction of actin levels in mouse testes. Cryosections of wild-type and GAR22β$^{-/-}$ testes were stained with fluorescent phalloidin and DRAQ5 red (nuclear staining) and then analyzed by confocal microscopy. In wild-type testes, actin was distributed throughout the seminiferous tubuli. Robust actin labeling can be seen both at the periphery and in the central region of single tubuli. In particular, in central tubular regions, actin accumulated in areas corresponding to spermatozoa heads (arrows). In GAR22β$^{-/-}$ testes, by contrast, the general level of actin was substantially reduced, with little or no actin around spermatozoa heads (arrows). Thin-lined boxes indicate the area enlarged in the thicker-lined boxes. Scale bars, 50 μm.

Video microscopy, wound-healing assay, and TIRF microscopy

For video microscopy, cells were plated onto 40-mm round glass coverslips (B16F1 cells were seeded on laminin-coated coverslips). Twenty-four hours later, coverslips were mounted in a FCS2 chamber heating system (Bioptechs, Butler, PA). To minimize focus drifts, an objective heater (Bioptechs) was used to eliminate the temperature gradient between chamber and oil immersion objective. The influence of GAR22β on the motility of B16F1 cells was determined through the analysis of parameters such as speed, persistence of movement, and directionality using the Dynamic Image Analysis System (Soll Technologies, Oakdale, LA). To analyze the ability of cells to migrate across a gap (wound-healing assay), control cells (untransfected NIH-3T3 or GAR22β$^{-/-}$ Sertoli cells) or cells expressing GAR22 variants were seeded in a cell culture insert (3.5×10^4 cells in 70 μl per chamber; ibidi, Munich, Germany) and grown until full confluent. After removal of the insert, cell migration was analyzed at given time points (0, 3, 6, 9, 12, and 24 h) or continuously for 24 h (in this case, images were acquired every 5 min). Phase contrast and epifluorescence images were acquired with an Axiovert 200 microscope (Carl Zeiss, Jena, Germany) using the most appropriate objective in combination with 1.6× or 2.5× Optovar optics. Images were recorded with a cooled, back-illuminated charge-coupled device (CCD) camera (Cascade 512B, used in conventional detection mode; Photometrics, Tucson, AZ) driven by IPLab Spectrum software (Scanalytics, Fairfax, VA).

TIRF microscopy was performed on an Axio Observer Z1 inverted microscope equipped with a motorized TIRF slider (Zeiss). Excitation of GFP and mCherry was done using 488- and 561-nm laser lines (both at 10% of their nominal output power), respectively. The depth of the evanescent field for both wavelengths was ~70 nm. Images were acquired every 2.5 s using an Evolve electron-multiplying CCD camera driven by ZEN software (Zeiss). For all experiments, exposure time, depth of the evanescent field, and electronic gain were kept constant.

Digital handling of the images was done using IPLab Spectrum, Graphic Converter, ImageJ (National Institutes of Health, Bethesda, MD), and Adobe Photoshop (Adobe Systems, San

Jose, CA). To improve figure clarity, when necessary, we adjusted the brightness and the contrast of the images and applied a sharpening filter.

Statistical analysis

All graphs and statistical analyses were done with Prism 5 (GraphPad Software, La Jolla, CA). Statistical analyses were done using the two-tailed Mann–Whitney nonparametric *U* test and rejecting the null hypothesis (the two groups have the same median values, i.e., they are not different) when $p > 0.05$. For the box-and-whiskers plots, the line in the middle of the box indicates the median, the top of the box indicates the 75th quartile, and the bottom of the box indicates the 25th quartile. Whiskers represent the 10th (lower) and 90th (upper) percentiles.

ACKNOWLEDGMENTS

We thank J. Weis (Institute of Neuropathology, RWTH Aachen, Aachen, Germany) for his help during the preliminary histological analysis of mouse testes. We also thank Xiaoying Wang for teaching us how to isolate Sertoli cells and A. Huttenlocher, A. Gudkov, R. Liem, T. Noetzel, and R. Tsien for kindly providing plasmids. We are grateful to T. Pfeffer for support with GAR22β$^{-/-}$ mouse generation and spermatozoa analysis. We thank H. Königs and S. Rütten for transmission electron microscopy/scanning electron microscopy and the personnel at the London Regional Proteomics Centre (www.lrpc.uwo.ca) for sample processing and protein identification by mass spectrometry. M.S. is a Lichtenberg-Professor of the Volkswagen Foundation. This work was supported by grants of the Deutsche Forschungsgemeinschaft to B.L. and M.Z. This work was also partly supported by the Interdisziplinäre Zentrum für Klinische Forschung Aachen (Project T1 to A.S.) and the START Programme (Project 01/05 to A.S.) of the Medical Faculty of RWTH Aachen University.

REFERENCES

Applewhite DA, Grode KD, Keller D, Zadeh AD, Slep KC, Rogers SL (2010). The spectraplakin Short stop is an actin-microtubule cross-linker that contributes to organization of the microtubule network. Mol Biol Cell 21, 1714–1724.

Ballestrem C, Wehrle-Haller B, Hinz B, Imhof BA (2000). Actin-dependent lamellipodia formation and microtubule-dependent tail retraction control-directed cell migration. Mol Biol Cell 11, 2999–3012.

Bellve AR, Cavicchia JC, Millette CF, O'Brien DA, Bhatnagar YM, Dym M (1977). Spermatogenic cells of the prepuberal mouse. Isolation and morphological characterization. J Cell Biol 74, 68–85.

Bershadsky AD, Vaisberg EA, Vasiliev JM (1991). Pseudopodial activity at the active edge of migrating fibroblast is decreased after drug-induced microtubule depolymerization. Cell Motil Cytoskeleton 19, 152–158.

Best A, Ahmed S, Kozma R, Lim L (1996). The Ras-related GTPase Rac1 binds tubulin. J Biol Chem 271, 3756–3762.

Bu W, Su LK (2001). Regulation of microtubule assembly by human EB1 family proteins. Oncogene 20, 3185–3192.

Byers TJ, Beggs AH, McNally EM, Kunkel LM (1995). Novel actin crosslinker superfamily member identified by a two step degenerate PCR procedure. FEBS Lett 368, 500–504.

Carlier MF, Pantaloni D (2007). Control of actin assembly dynamics in cell motility. J Biol Chem 282, 23005–23009.

Daub H, Gevaert K, Vandekerckhove J, Sobel A, Hall A (2001). Rac/Cdc42 and p65PAK regulate the microtubule-destabilizing protein stathmin through phosphorylation at serine 16. J Biol Chem 276, 1677–1680.

Disanza A, Steffen A, Hertzog M, Frittoli E, Rottner K, Scita G (2005). Actin polymerization machinery: the finish line of signaling networks, the starting point of cellular movement. Cell Mol Life Sci 62, 955–970.

Dunn GA, Zicha D, Fraylich PE (1997). Rapid, microtubule-dependent fluctuations of the cell margin. J Cell Sci 110, 3091–3098.

Fukata M, Watanabe T, Noritake J, Nakagawa M, Yamaga M, Kuroda S, Matsuura Y, Iwamatsu A, Perez F, Kaibuchi K (2002). Rac1 and Cdc42 capture microtubules through IQGAP1 and CLIP-170. Cell 109, 873–885.

Gamper I, Koh KR, Ruau D, Ullrich K, Bartunkova J, Piroth D, Hacker C, Bartunek P, Zenke M (2009). GAR22: a novel target gene of thyroid hormone receptor causes growth inhibition in human erythroid cells. Exp Hematol 37, 539–548.e4.

Goldman RD (1971). The role of three cytoplasmic fibers in BHK-21 cell motility. I. Microtubules and the effects of colchicine. J Cell Biol 51, 752–762.

Goriounov D, Leung CL, Liem RK (2003). Protein products of human Gas2-related genes on chromosomes 17 and 22 (hGAR17 and hGAR22) associate with both microfilaments and microtubules. J Cell Sci 116, 1045–1058.

Gungor-Ordueri NE, Tang EI, Celik-Ozenci C, Cheng CY (2014). Ezrin is an actin binding protein that regulates sertoli cell and spermatid adhesion during spermatogenesis. Endocrinology 155, 3981–3995.

Guo L, Degenstein L, Dowling J, Yu QC, Wollmann R, Perman B, Fuchs E (1995). Gene targeting of BPAG1: abnormalities in mechanical strength and cell migration in stratified epithelia and neurologic degeneration. Cell 81, 233–243.

Honnappa S, Gouveia SM, Weisbrich A, Damberger FF, Bhavesh NS, Jawhari H, Grigoriev I, van Rijssel FJ, Buey RM, Lawera A, *et al*. (2009). An EB1-binding motif acts as a microtubule tip localization signal. Cell 138, 366–376.

Ishizaki T, Morishima Y, Okamoto M, Furuyashiki T, Kato T, Narumiya S (2001). Coordination of microtubules and the actin cytoskeleton by the Rho effector mDia1. Nat Cell Biol 3, 8–14.

Jefferson JJ, Ciatto C, Shapiro L, Liem RK (2007). Structural analysis of the plakin domain of bullous pemphigoid antigen1 (BPAG1) suggests that plakins are members of the spectrin superfamily. J Mol Biol 366, 244–257.

Jiang K, Toedt G, Montenegro Gouveia S, Davey NE, Hua S, van der Vaart B, Grigoriev I, Larsen J, Pedersen LB, Bezstarosti K, *et al*. (2012). A Proteome-wide screen for mammalian SxIP motif-containing microtubule plus-end tracking proteins. Curr Biol 22, 1800–1807.

Kalebic N, Sorrentino S, Perlas E, Bolasco G, Martinez C, Heppenstall PA (2013). alphaTAT1 is the major alpha-tubulin acetyltransferase in mice. Nat Commun 4, 1962.

Kaverina I, Krylyshkina O, Small JV (1999). Microtubule targeting of substrate contacts promotes their relaxation and dissociation. J Cell Biol 146, 1033–1044.

Kaverina I, Rottner K, Small JV (1998). Targeting, capture, and stabilization of microtubules at early focal adhesions. J Cell Biol 142, 181–190.

Kodama A, Karakesisoglou I, Wong E, Vaezi A, Fuchs E (2003). ACF7: an essential integrator of microtubule dynamics. Cell 115, 343–354.

Krylyshkina O, Kaverina I, Kranewitter W, Steffen W, Alonso MC, Cross RA, Small JV (2002). Modulation of substrate adhesion dynamics via microtubule targeting requires kinesin-1. J Cell Biol 156, 349–359.

Li MW, Xiao X, Mruk DD, Lam YL, Lee WM, Lui WY, Bonanomi M, Silvestrini B, Cheng CY (2011). Actin-binding protein drebrin E is involved in junction dynamics during spermatogenesis. Spermatogenesis 1, 123–136.

Liao G, Nagasaki T, Gundersen GG (1995). Low concentrations of nocodazole interfere with fibroblast locomotion without significantly affecting microtubule level: implications for the role of dynamic microtubules in cell locomotion. J Cell Sci 108, 3473–3483.

Lie PP, Chan AY, Mruk DD, Lee WM, Cheng CY (2010b). Restricted Arp3 expression in the testis prevents blood-testis barrier disruption during junction restructuring at spermatogenesis. Proc Natl Acad Sci USA 107, 11411–11416.

Lie PP, Mruk DD, Lee WM, Cheng CY (2009). Epidermal growth factor receptor pathway substrate 8 (Eps8) is a novel regulator of cell adhesion and the blood-testis barrier integrity in the seminiferous epithelium. FASEB J 23, 2555–2567.

Lie PP, Mruk DD, Lee WM, Cheng CY (2010a). Cytoskeletal dynamics and spermatogenesis. Philos Trans R Soc Lond B Biol Sci 365, 1581–1592.

Ligon LA, Shelly SS, Tokito M, Holzbaur EL (2003). The microtubule plus-end proteins EB1 and dynactin have differential effects on microtubule polymerization. Mol Biol Cell 14, 1405–1417.

Mahony D, Karunaratne S, Rothnagel JA (2002). Improved detection of lacZ reporter gene expression in transgenic epithelia by immunofluorescence microscopy. Exp Dermatol 11, 153–158.

Mierke CT, Kollmannsberger P, Zitterbart DP, Diez G, Koch TM, Marg S, Ziegler WH, Goldmann WH, Fabry B (2010). Vinculin facilitates cell invasion into three-dimensional collagen matrices. J Biol Chem 285, 13121–13130.

Mikhailov A, Gundersen GG (1998). Relationship between microtubule dynamics and lamellipodium formation revealed by direct imaging of

microtubules in cells treated with nocodazole or taxol. Cell Motil Cytoskeleton 41, 325–340.
O'Donnell L, O'Bryan MK (2014). Microtubules and spermatogenesis. Semin Cell Dev Biol 30, 45–54.
Okuda T, Matsuda S, Nakatsugawa S, Ichigotani Y, Iwahashi N, Takahashi M, Ishigaki T, Hamaguchi M (1999). Molecular cloning of macrophin, a human homologue of Drosophila kakapo with a close structural similarity to plectin and dystrophin. Biochem Biophys Res Commun 264, 568–574.
Ossovskaya VS, Mazo IA, Chernov MV, Chernova OB, Strezoska Z, Kondratov R, Stark GR, Chumakov PM, Gudkov AV (1996). Use of genetic suppressor elements to dissect distinct biological effects of separate p53 domains. Proc Natl Acad Sci USA 93, 10309–10314.
Palazzo AF, Cook TA, Alberts AS, Gundersen GG (2001). mDia mediates Rho-regulated formation and orientation of stable microtubules. Nat Cell Biol 3, 723–729.
Pfister AS, Hadjihannas MV, Rohrig W, Schambony A, Behrens J (2012). Amer2 protein interacts with EB1 protein and adenomatous polyposis coli (APC) and controls microtubule stability and cell migration. J Biol Chem 287, 35333–35340.
Qian X, Mruk DD, Cheng YH, Tang EI, Han D, Lee WM, Wong EW, Cheng CY (2014). Actin binding proteins, spermatid transport and spermiation. Semin Cell Dev Biol 30, 75–85.
Qian X, Mruk DD, Wong EW, Lie PP, Cheng CY (2013). Palladin is a regulator of actin filament bundles at the ectoplasmic specialization in adult rat testes. Endocrinology 154, 1907–1920.
Rodriguez OC, Schaefer AW, Mandato CA, Forscher P, Bement WM, Waterman-Storer CM (2003). Conserved microtubule-actin interactions in cell movement and morphogenesis. Nat Cell Biol 5, 599–609.
Sanchez-Soriano N, Travis M, Dajas-Bailador F, Goncalves-Pimentel C, Whitmarsh AJ, Prokop A (2009). Mouse ACF7 and drosophila short stop modulate filopodia formation and microtubule organisation during neuronal growth. J Cell Sci 122, 2534–2542.
Schober JM, Cain JM, Komarova YA, Borisy GG (2009). Migration and actin protrusion in melanoma cells are regulated by EB1 protein. Cancer Lett 284, 30–36.
Schober JM, Kwon G, Jayne D, Cain JM (2012). The microtubule-associated protein EB1 maintains cell polarity through activation of protein kinase C. Biochem Biophys Res Commun 417, 67–72.
Sechi AS, Wehland J (2004). ENA/VASP proteins: multifunctional regulators of actin cytoskeleton dynamics. Front Biosci 9, 1294–1310.
Slep KC, Rogers SL, Elliott SL, Ohkura H, Kolodziej PA, Vale RD (2005). Structural determinants for EB1-mediated recruitment of APC and spectraplakins to the microtubule plus end. J Cell Biol 168, 587–598.
Small JV, Stradal T, Vignal E, Rottner K (2002). The lamellipodium: where motility begins. Trends Cell Biol 12, 112–120.
Stroud MJ, Nazgiewicz A, McKenzie EA, Wang Y, Kammerer RA, Ballestrem C (2014). GAS2-like proteins mediate communication between microtubules and actin through interactions with end-binding proteins. J Cell Sci 127, 2672–2682.
Su W, Mruk DD, Lie PP, Lui WY, Cheng CY (2012). Filamin A is a regulator of blood-testis barrier assembly during postnatal development in the rat testis. Endocrinology 153, 5023–5035.
Sun D, Leung CL, Liem RK (2001). Characterization of the microtubule binding domain of microtubule actin crosslinking factor (MACF): identification of a novel group of microtubule associated proteins. J Cell Sci 114, 161–172.
Vaid KS, Guttman JA, Singaraja RR, Vogl AW (2007). A kinesin is present at unique sertoli/spermatid adherens junctions in rat and mouse testes. Biol Reprod 77, 1037–1048.
Vasiliev JM, Gelfand IM, Domnina LV, Ivanova OY, Komm SG, Olshevskaja LV (1970). Effect of colcemid on the locomotory behaviour of fibroblasts. J Embryol Exp Morphol 24, 625–640.
Veitinger S, Veitinger T, Cainarca S, Fluegge D, Engelhardt CH, Lohmer S, Hatt H, Corazza S, Spehr J, Neuhaus EM, Spehr M (2011). Purinergic signalling mobilizes mitochondrial Ca^{2+} in mouse Sertoli cells. J Physiol 589, 5033–5055.
Waterman-Storer CM, Worthylake RA, Liu BP, Burridge K, Salmon ED (1999). Microtubule growth activates Rac1 to promote lamellipodial protrusion in fibroblasts. Nat Cell Biol 1, 45–50.
Wen Y, Eng CH, Schmoranzer J, Cabrera-Poch N, Morris EJ, Chen M, Wallar BJ, Alberts AS, Gundersen GG (2004). EB1 and APC bind to mDia to stabilize microtubules downstream of Rho and promote cell migration. Nat Cell Biol 6, 820–830.
Wong EW, Mruk DD, Lee WM, Cheng CY (2010). Regulation of blood-testis barrier dynamics by TGF-beta3 is a Cdc42-dependent protein trafficking event. Proc Natl Acad Sci USA 107, 11399–11404.
Wu X, Kodama A, Fuchs E (2008). ACF7 regulates cytoskeletal-focal adhesion dynamics and migration and has ATPase activity. Cell 135, 137–148.
Würflinger T, Gamper I, Aach T, Sechi AS (2011). Automated segmentation and tracking for large-scale analysis of focal adhesion dynamics. J Microsc 241, 37–53.
Yamazaki D, Suetsugu S, Miki H, Kataoka Y, Nishikawa S, Fujiwara T, Yoshida N, Takenawa T (2003). WAVE2 is required for directed cell migration and cardiovascular development. Nature 424, 452–456.
Yeung CH, Sonnenberg-Riethmacher E, Cooper TG (1999). Infertile spermatozoa of c-ros tyrosine kinase receptor knockout mice show flagellar angulation and maturational defects in cell volume regulatory mechanisms. Biol Reprod 61, 1062–1069.
Young JS, Guttman JA, Vaid KS, Shahinian H, Vogl AW (2009). Cortactin (CTTN), N-WASP (WASL), and clathrin (CLTC) are present at podosome-like tubulobulbar complexes in the rat testis. Biol Reprod 80, 153–161.